
How Controlling the Variance can Improve Training Stability of Sparsely Activated DNNs and CNNs

Emily Dent, Jared Tanner

Mathematical Institute
University of Oxford
Oxford, UK

emily.dent@maths.ox.ac.uk, jared.tanner@maths.ox.ac.uk

Abstract

The intermediate layers of deep networks can be characterised as a Gaussian process, in particular the Edge-of-Chaos (EoC) initialisation strategy prescribes the limiting covariance matrix of the Gaussian process. Here we show that the under-utilised chosen variance of the Gaussian process is important in the training of deep networks with sparsity inducing activation, such as a shifted and clipped ReLU, $\text{CReLU}_{\tau,m}(x) = \min(\max(x - \tau, 0), m)$. Specifically, initialisations leading to larger fixed Gaussian process variances, allow for improved expressivity with activation sparsity as large as 90% in DNNs and CNNs, and generally improve the stability of the training process. Enabling full, or near full, accuracy at such high levels of sparsity in the hidden layers suggests a promising mechanism to reduce the energy consumption of machine learning models involving fully connected layers.

1 Introduction

Improving the computational efficiency of ML models is an area of intense investigation Menghani (2023) in order to both reduce the overall power consumption of these models and to enable their greater deployment on edge-devices. The most prevalent techniques include: compact architectures design Howard et al. (2017), low-rank weight matrices Osawa et al. (2017) such as in the popular LoRA framework Hu et al. (2021), low-precision quantisation Weng (2023) such as in recent GPU hardware, and pruning weight matrices such as Blalock et al. (2020) see references therein and Section 1.1. Here the focus is on a less studied method to improve computational efficiency, that of having highly sparse hidden layers which can be achieved with nonlinear activations that induce the desired level of sparsity Price et al. (2024). This sparse hidden layer framework benefits from automatic computational efficiency gains by requiring only the non-zero hidden layer values and associated columns of the weight matrices which can be trivially implemented in existing hardware.

Training of DNNs and CNNs with activations that induce high degrees of sparsity, e.g. 85% and greater, raises some novel initialisation challenges and nonlinear activation designs Price et al. (2024). In its simplest form, the Edge-of-Chaos (EoC) theory considers networks with pre-activation hidden layers given by $h^{(\ell)} = W^{(\ell)}\phi(h^{(\ell-1)}) + b^{(\ell)}$ and studies properties of $h^{(\ell)}$ as a function of $\phi(\cdot)$ and the initialisation of the weights and biases. In particular, EoC theory describes the limiting distribution of $h^{(\ell)}$ as a mean zero Gaussian process with variance $\mathbb{E} [h_i^{(\ell)}]^2$ and explains how the variance evolves through layers ℓ . This manuscript extends the EoC theory to the study of activations which are zero around the origin by showing for exemplar $\phi(\cdot)$ with control of the parameter $\mathbb{E} [h_i^{(\ell)}]^2$ it is possible to improve the training accuracy and stability of networks and enable even greater sparsity.

Inspired by the infinite width limit Gaussian behaviour of the hidden layers, $h_i^{(\ell)} \sim \mathcal{N}(0, q^{(\ell)})$, and the supposition that the largest entries are most important, consider activations $\phi(\cdot)$ for which $\phi(z) = 0$ for $|z| \leq \tau$, where z contains the active outputs h and τ is a parameter determining the level of sparsity. For clarity of exposition we focus on two illustrative examples as in Price et al. (2024), $\text{CReLU}_{\tau,m}$ and $\text{CST}_{\tau,m}$.

$$\text{CReLU}_{\tau,m}(x) = \begin{cases} 0, & \text{if } x < \tau \\ x - \tau, & \text{if } \tau \leq x \leq \tau + m \\ m, & \text{if } x > \tau + m, \end{cases} \quad (1)$$

$$\text{CST}_{\tau,m}(x) = \begin{cases} 0, & \text{if } |x| < \tau \\ x - \text{sign}(x)\tau, & \text{if } \tau \leq |x| \leq \tau + m \\ \text{sign}(x)m, & \text{if } |x| > \tau + m. \end{cases} \quad (2)$$

Here m is a hyper parameter chosen to balance the expressivity and ease of training for large valued τ .

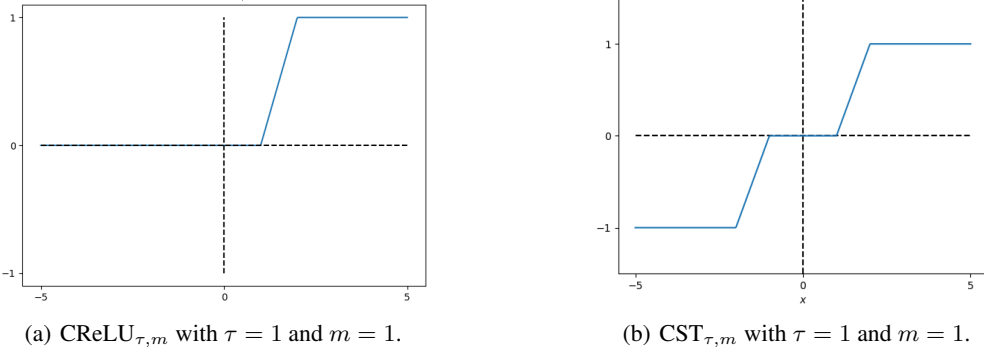


Figure 1: Non-linear activations $\text{CReLU}_{\tau,m}$, (a), and $\text{CST}_{\tau,m}$, (b), as defined in (1), (2) respectively, with $\tau = 1$ and $m = 1$.

The phenomena of training instability occurs for other similar activations which are zero around the origin. Difficulties in training occur for the sparsifying activation functions as a result of instability in the empirical $\tilde{q}^{(\ell)}$. The EoC theory typically advocates that $\mathbb{E} [h_i^{(\ell)2}]$ converges independently to a non-zero limit q^* or decays slowly to zero. However, here a new phenomena is shown whereby increasing q^* both reduces the sensitivity of the scale of the back-propagated errors to the empirical hidden layer variance, as well as improves the stability of $\tilde{q}^{(\ell)}$ itself.

Experiments are shown whereby increasing q^* allows more consistent training of DNNs and CNNs with high sparsity levels, achieving sparsity up to 90%.

1.1 Related Work

There is a range of related work which mathematically characterises the behaviour of the hidden layers and proposes methods to improve stability and training of large neural networks. As mentioned previously Price et al. (2024) pioneered the results extended here. The remainder of this section reviews other methods to further stabilize information propagation on the Edge-of-Chaos.

Traditional EoC theory presumes a rapid and stable convergence of $\mathbb{E} [h_i^{(\ell)2}]$ to q^* in depth and then focuses on higher order phenomena. In particular, through concentration of *all* singular values of the input-output Jacobian towards 1, see Pennington et al. (2017, 2018); Xiao et al. (2018). Specifically, these works analyse the variance of the spectrum of the input-output Jacobian JJ^T , denoted as σ_{JJ^T} . To better concentrate the spectrum of JJ^T they propose methods so that $\sigma_{JJ^T} \rightarrow 0$. The first approach was in Pennington et al. (2018) where they propose taking $q^* \rightarrow 0$ to cause $\sigma_{JJ^T} \rightarrow 0$. In Martens et al. (2021); Roberts & Yaida (2022); Murray et al. (2022) they also advocate taking $q^* \rightarrow 0$, for certain activation functions. Another methodology proposed in Murray et al. (2022);

Martens et al. (2021) shows that information propagation is improved through a linearized region around the origin of the activation function. These mentioned works are to the best of our knowledge the only other cases to consider varying q^* , all of which only consider the limit of a decreasing, or arbitrarily chosen q^* . A further in depth analysis of the EoC and additional finite-width corrections can be found in Yaida (2020); Roberts & Yaida (2022); Hanin (2023).

Extensions to the EoC initialisation have been explored for other architectures including ResNets Yang & Schoenholz (2017) and Recurrent Neural Networks Xie et al. (2025). The perhaps natural extension of this work to ResNets is not explored for the precise reason that the skip connections would negate the induced sparsity in the activation function, and therefore the proposed efficiency improvements. Transformer architectures are also not considered here, as they are a separate line of analysis with additional complexity.

There are a range of motivations for the particular case of activation sparsity, one such property is the immediate computational reducibility for entire rows in the matrix multiplication. An incentivizing example for this efficiency improvement comes from the identification of naturally occurring sparsity leading to brain efficiency improvements in neuroscience, Attwell & Laughlin (2001). Separately, sparsity is also shown to improve the ability of models to generalize and learn Frankle & Carbin (2018); Muthukumar & Sulam (2023); Awasthi et al. (2024); a phenomenon colloquially known as the *lottery ticket*. Due to this intuition, some recent work considers activation sparsity in attention, see Zhang et al. (2024); Luo et al. (2025); You et al. (2025); in You et al. (2025) they find competitive activation sparsity up to 92%, however these works are largely empirical in nature.

There is also some parallel literature which is related, but not the main focus of this work. One of these is the study of high variance weight initialisation leading to faster training, as a *lazy training* method, this was first mentioned in Chizat et al. (2019), and has further been explored in Dominé et al. (2023, 2024); in this work, as a result of increasing q^* on the EoC, the initial variance of the weights is increased. Another linked line of work is gradient clipping, as the exemplar activation function in this work, CReLU $_{\tau,m}$, could be interpreted as a method for naturally encouraging gradient clipping; however it should be noted that CReLU $_{\tau,m}$ is but a particularly simple example, which has the essential property of bounding ReLU. Gradient clipping is used to improve training stability, as well as to encourage privacy in Differential Privacy algorithms; see Pascanu et al. (2013); Zhang et al. (2019); Mai & Johansson (2021); Marshall et al. (2024); Bombari et al. (2025).

Here, we focus on the mathematical motivations behind the parameter choices, and show that increasing q^* is a technique to achieve stable and highly sparsifying activation functions - experiments then show proof of concept for this work.

2 Edge-of-Chaos

The following first considers a review of the EoC theory. Explicitly considering the limiting behaviour for Deep Neural Networks (DNNs), a DNN has hidden layers with activation function ϕ given by,

$$h_i^{(\ell)} = \sum_{j=1}^{N_l} W_{ij}^{(\ell)} x_j^{(\ell-1)} + b_i^{(\ell)}, \quad (3)$$

$$x_i^{(\ell)} = \phi\left(h_i^{(\ell)}\right),$$

where ℓ is the layer number, N_ℓ is the width of layer ℓ , and $W_{ij}^{(\ell)}$ and $b_i^{(\ell)}$ are the weights and biases for layer ℓ respectively. Much of the analysis for Convolutional Neural Networks (CNNs) is similar, Xiao et al. (2018). The Edge-of-Chaos initialisation is then given by $W_{ij}^{(\ell)} \sim \mathcal{N}\left(0, \frac{\sigma_w^2}{N_\ell}\right)$ and $b_i^{(\ell)} \sim \mathcal{N}(0, \sigma_b^2)$, where σ_w^2 and σ_b^2 are selected according to roles that are known to improve information propagation in deep neural networks, Schoenholz et al. (2017).

In the infinite width limit these hidden layers are known to behave as Gaussian random variables Neal (1996); Matthews et al. (2018); Lee et al. (2018), further Poole et al. (2016) characterised this initialisation admitting hidden layers with distribution $h_i^{(\ell)} \sim \mathcal{N}(0, q^{(\ell)})$, where $q^{(\ell)}$ evolves with

the iterative mapping,

$$q^{(\ell)} = V\left(q^{(\ell-1)}\right) \quad (4)$$

$$:= \sigma_w^2 \int_{\mathbb{R}} \left[\phi\left(\sqrt{q^{(\ell-1)}} z\right) \right]^2 \gamma(dz) + \sigma_b^2, \quad (5)$$

where $\gamma(dz) = e^{-z^2/2}/\sqrt{2\pi}$. In a stable regime, $V(q)$ admits a fixed point q^* , and for $V'(q^*) < 1$, $V(q^{(\ell)}) \rightarrow q^*$ as $l \rightarrow \infty$. As such for CReLU $_{\tau,m}$ to induce sparsity level s set $\hat{\tau} = \sqrt{q^*} \Phi^{-1}(s)$.

Further consider the correlation map between two inputs,

$$\rho^{(\ell)} = R_{\phi}(\rho^{(\ell-1)}) := \frac{1}{q^*} \left(\sigma_w^2 \int_{\mathbb{R}} \int_{\mathbb{R}} \phi(u_1) \phi(u_2) \gamma(dz_1) \gamma(dz_2) + \sigma_b^2 \right), \quad (6)$$

where,

$$u_1 = \sqrt{q^*} z_1, \quad (7)$$

$$u_2 = \sqrt{q^*} \left(\rho^{(\ell-1)} z_1 + \sqrt{1 - \rho^{(\ell-1)}^2} z_2 \right), \quad (8)$$

$$\rho^{(\ell-1)} = q_{ab}^{(\ell-1)} / \sqrt{q_{aa}^{(\ell-1)} q_{bb}^{(\ell-1)}}, \quad (9)$$

$\rho^{(\ell-1)}$ is the correlation at layer $l-1$, and z_1, z_2 are independent Gaussian random variables. The correlation map (6) will always admit a fixed point at $\rho = 1$. The EoC initialisation is defined by the derivative of the correlation map R_{ϕ} at 1;

$$\chi_1(q^*) = R'_{\phi}(1) := \sigma_w^2 \int [\phi'(\sqrt{q^*} z)]^2 \gamma(dz), \quad (10)$$

being equal to 1. After an arbitrary choice of q^* , typically $q^* = 1$, this is achieved by then setting σ_w^2 such that χ_1 is 1 in (10), consequently σ_b^2 is chosen such that $V(q^*) = q^*$ as in (5). $\chi_1(q^*)$ is also equal to the (first-order) multiplicative perturbation across a single layer, Poole et al. (2016); therefore, $\chi_1(q^*) > 1$ results in exploding perturbations and in deeper neural networks $\chi_1(q^*) < 1$ is overly conservative, driving the network towards a constant function, whereas setting $\chi_1(q^*) = 1$, the Edge-of-Chaos, results in stable perturbations, and was shown to prevent vanishing/exploding gradients Schoenholz et al. (2017).

To show how χ_1 relates to the scaling of perturbations across a single layer in training, the second moment of the errors distribution, $\tilde{v}^{(\ell)} = \mathbb{E}[(\delta_i^{(\ell)})^2]$ was shown in Schoenholz et al. (2017) to evolve according to a recurrent relation dependent on χ_1 ,

$$\tilde{v}^{(\ell)} = \tilde{v}^{(\ell+1)} \frac{N_{\ell+1}}{N_{\ell}} \chi_1. \quad (11)$$

Therefore for a network where $N_{\ell} = N \forall l \in \{1, \dots, L\}$, $\tilde{v}^{(\ell)} = \tilde{v}^{(0)} (\chi_1)^{\ell}$.

Typically, the literature assumes $q^{(\ell)} \rightarrow q^*$ almost immediately and so χ_1 is as in (10). However, this is not reasonably the case in practice, and $q^{(\ell)}$ is observed to vary stochastically around the point q^* .

$$\chi_1(q^{(\ell)}) := \sigma_w^2 \int [\phi'(\sqrt{q^{(\ell)}} z)]^2 \gamma(dz), \quad (12)$$

is a function of $q^{(\ell)}$, and so any lack of symmetry about q^* in the dependence of χ_1 as a function of $q^{(\ell)}$ may create a growth in $\tilde{v}^{(\ell)} = \prod_{\ell=1}^L \chi_1(q^{(\ell)})$ which can be exponential in depth and tells us directly about the accumulated growth of errors through the network. Further study of χ_1 can be found in Poole et al. (2016); Schoenholz et al. (2017); Xiao et al. (2018), see also Section A.

2.1 Main Contributions

The essential reasons for the loss of stability for training CReLU $_{\tau,m}$ for large m are shown in Figure 2. Nearly identical behaviour is observed for CST $_{\tau,m}$, see Section B. As m increases, in a

local region around the fixed point q^* the slope of the variance map increases, to the point where for some larger values of m global stability of these is lost. Moreover, there is also an appearance of a second fixed point. This appearance of a second fixed point is the more obvious failure in a network as χ_1 would be greater than 1 at this second fixed point. Further, Price et al. (2024) found a more subtle issue of training failure even with global stability would occur in the large width limit. This second failure is a result of a strong loss of symmetry in $V(q)$ about the fixed point q^* for these larger values of m , which causes $\chi_1(q^{(\ell)})$ to have a bias towards values greater than one. All issues for $V_{\text{CReLU}_{\tau,m}}$ are only exacerbated for $V_{\text{CST}_{\tau,m}}$, see Section B.

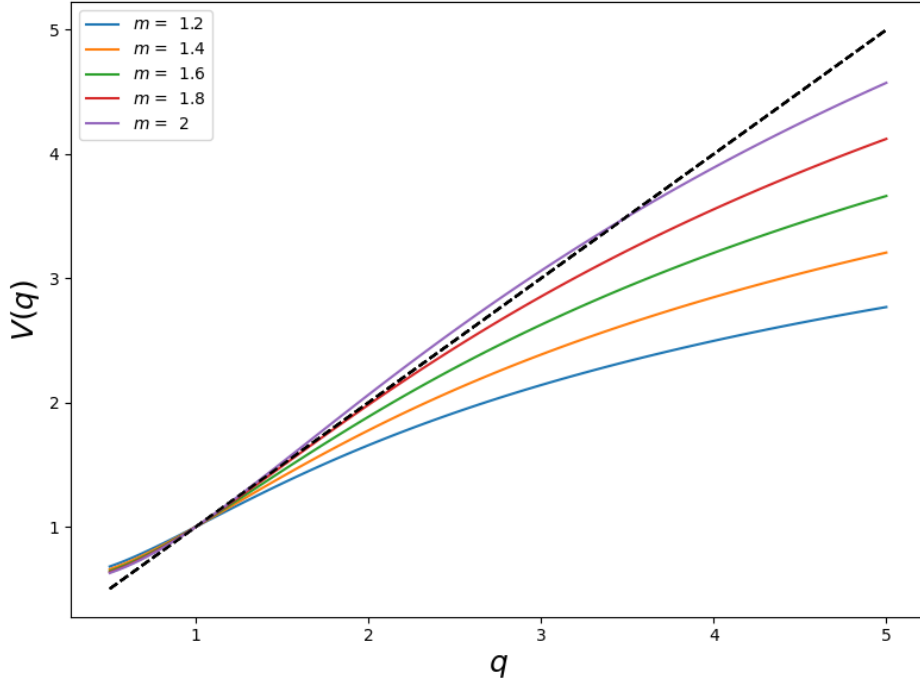


Figure 2: $V_{\text{CReLU}_{\tau,m}}(q)$, for $q^* = 1$, $s = 0.85$ with varying values of $m = 1.2, 1.4, 1.6, 1.8, 2.0$, with vertical axis is $V(q)$ and horizontal axis q . As m increases $V'_{\text{CReLU}_{\tau,m}}(q) \rightarrow 1$ and $V''_{\text{CReLU}_{\tau,m}}(q)$ exceeds zero, resulting in a second fixed point at $q \approx 3.5$ for $m = 2.0$.

As mentioned, in the deterministic view of the iterative variance map, $q^{(\ell)}$ will always converge to the fixed point under the Law of Large Numbers where $V'(q^*) < 1$. However in actuality $q^{(\ell)}$ has variability due to the infinite limit assumption, and is a random variable itself. This was extensively explored in Roberts & Yaida (2022), where the appearance of $V''(q^*)$ also appears in the next-leading-order term. For larger values of $V''(q^*)$, where there is a strong loss of symmetry around the fixed point, the iterative map cannot sufficiently control the perturbations, see Figure 2. The perturbations around q^* are then asymmetrical, resulting in an unstable regime for the variance of the hidden layers $q^{(\ell)}$, since the $\prod_{\ell=1}^L \chi_1(q^{(\ell)})$ accumulates values biased to be greater than 1, and grows exponentially with depth. Here the curvature, $V''(q^*)$ is used as a heuristic for the lack of symmetry, the curvature is similarly used for the next-leading-order term in considering the finite dimensional correction as in Roberts & Yaida (2022) (Chapters 4 and 5).

This loss of symmetry constrains how large m can be selected which limits, the expressivity of the network before instability occurs, and therefore the lack of trainability found in Price et al. (2024). Firstly, by improving the symmetry of the variance map; and secondly by reducing the sensitivity of $\chi_1(q)$ to q . These two approaches are shown in Section 2.1.1 and Section 2.1.3 to occur by increasing q^* . Section 2.1.2 further shows that increasing q^* can decrease the finite dimensional corrections.

2.1.1 Concentrating $q^{(\ell)}$

To consider how to improve the concentration of $q^{(\ell)}$, consider the variance maps $V(q)$. To first remove the certain instability arising from $V'(q^*) > 1$, as in Price et al. (2024), see

$$V'_{\text{CReLU}_{\tau,m}}(q) = \sigma_w^2 \left[\frac{1}{2} \text{erf} \left(\frac{\tau+m}{\sqrt{2q}} \right) - \frac{1}{2} \text{erf} \left(\frac{\tau}{\sqrt{2q}} \right) - \frac{m}{\sqrt{2\pi}q} \exp \left(-\frac{(\tau+m)^2}{2q} \right) \right]. \quad (13)$$

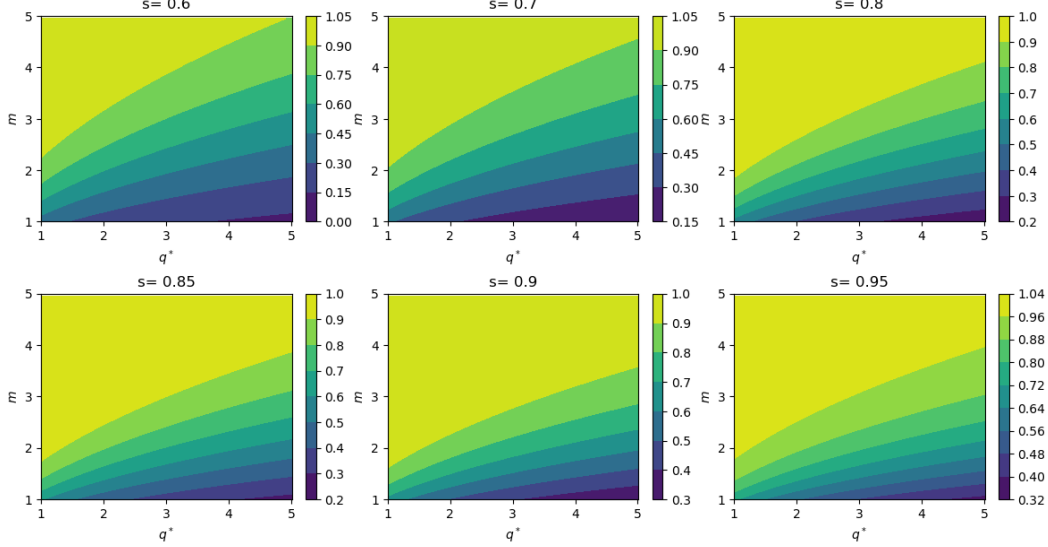


Figure 3: $V'_{\text{CReLU}_{\tau,m}}(q^*)$ for a range of $s = \{0.6, 0.7, 0.8, 0.85, 0.9, 0.95\}$, the plots of these six sparsities are from left to right then top to bottom, with horizontal axis q^* and vertical axis m . For fixed value m by increasing q^* , $V'_{\text{CReLU}_{\tau,m}}(q^*)$ reduces, this holds for all six sparsity levels.

Figure 3 shows that by increasing q^* , $V'_{\text{CReLU}_{\tau,m}}(q^*)$ decreases for a fixed sparsity and maximum value, m - and so we can regain global stability.

As mentioned previously, to control the loss of symmetry even where global stability occurs in the infinite width limit consider $V''(q^*)$. The expression for $V''_{\text{CReLU}_{\tau,m}}(q^*)$ is,

$$V''_{\text{CReLU}_{\tau,m}}(q) = \frac{\sigma_w^2}{\sqrt{8\pi}q^5} \exp \left(-\frac{(\tau+m)^2}{2q} \right) \left[q\tau \exp \left(\frac{2m\tau + \tau^2}{2q} \right) - q\tau - m(\tau+m)^2 \right]. \quad (14)$$

The exact derivation for $V''_{\text{CReLU}_{\tau,m}}(q)$ is uninformative, for interest see Section B.

Figure 4 further shows that for a fixed sparsity and maximum value m , increasing q^* decreases the curvature of the variance map for the chosen activation functions - further stabilizing the initialisation.

2.1.2 Finite Dimensional Correction

In Roberts & Yaida (2022), there is the additional consideration of the finite dimensional correction of the variance map. Let $\tilde{q}^{(\ell)}$ be the the finite dimensionally corrected variance, then the mean variance is $q^{(\ell)}$ which the dynamics of are known explicitly from the variance map, $V(\cdot)$. In particular, consider the variance $\tilde{q}^{(\ell)}$ and the fourth moment $r^{(\ell)}$ of the hidden layers as an infinite series of sub-leading order corrections. That is,

$$\tilde{q}^{(\ell)} = \tilde{q}^{\{0\}(\ell)} + \frac{1}{n_{l-1}} \tilde{q}^{\{1\}(\ell)} + \mathcal{O} \left(\frac{1}{n^2} \right), \quad (15)$$

$$r^{(\ell)} = r^{\{0\}(\ell)} + \frac{1}{n_{l-1}} r^{\{1\}(\ell)} + \mathcal{O} \left(\frac{1}{n^2} \right). \quad (16)$$

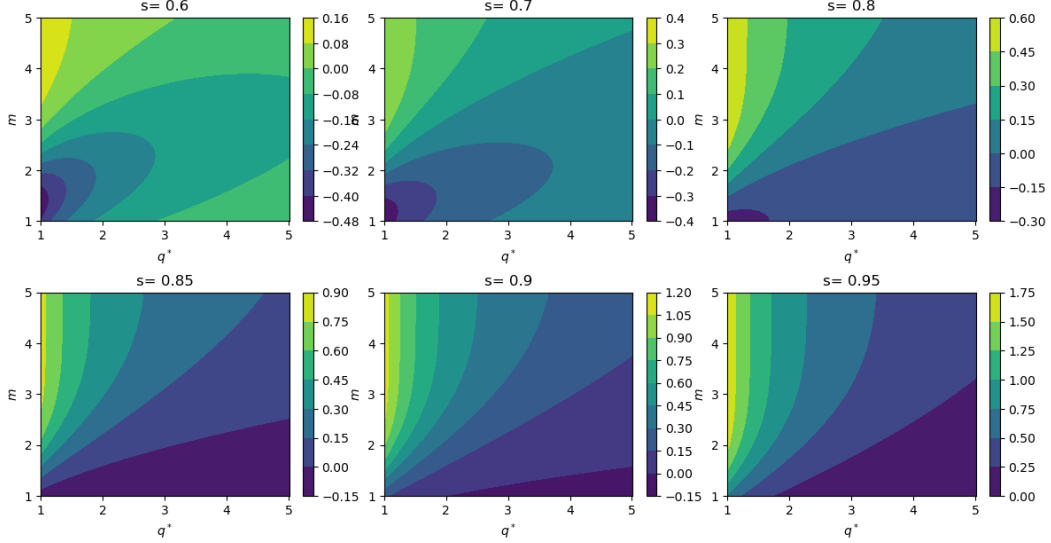


Figure 4: $V''_{\text{ReLU}_{\tau,m}}(q^*)$, for a range of $s = \{0.6, 0.7, 0.8, 0.85, 0.9, 0.95\}$, the plots of these six sparsities are from left to right then top to bottom, with horizontal axis q^* and vertical axis m . For high sparsity levels $s = \{0.85, 0.9, 0.95\}$, and fixed value m by increasing q^* , $V''_{\text{ReLU}_{\tau,m}}(q^*)$ reduces. For lower sparsity levels $s = \{0.6, 0.7, 0.8\}$ with larger values of m that by increasing q^* there is again a reduction in $V''_{\text{ReLU}_{\tau,m}}(q^*)$.

Denote $\tilde{q}^{\{1\}(\ell)}$ as the next-leading-order metric, which is the first-order correction to the variance. Where $r^{(\ell)}$ describes the size of fluctuations away from the mean variance $q^{(\ell)}$, as it controls the near-Gaussianity of the layer distribution (it is the leading deviation from Gaussianity). Note, the leading order term to $\tilde{q}^{(\ell)}$ fully describes the infinite-width limit to the pre-activation distribution,

$$q^{(\ell)} = \tilde{q}^{\{0\}(\ell)}. \quad (17)$$

Now introducing the operator for ease of notation,

$$\langle f(z) \rangle_q = \frac{1}{\sqrt{2\pi q}} \int_{\mathbb{R}} f(z) e^{-\frac{z^2}{q}} dz. \quad (18)$$

In Roberts & Yaida (2022) they find the equivalent following recursions,

$$q^{(\ell+1)} = V\left(q^{(\ell)}\right), \quad (19)$$

$$r^{(\ell+1)} = V'\left(q^{(\ell)}\right)^2 r^{(\ell)} + \sigma_w^4 \left(\langle \phi^4(z) \rangle_{q^{(\ell)}} - \langle \phi^2(z) \rangle_{q^{(\ell)}}^2 \right), \quad (20)$$

$$\tilde{q}^{\{1\}(\ell+1)} = V'\left(q^{(\ell)}\right) \tilde{q}^{\{1\}(\ell)} + \frac{1}{2} V''\left(q^{(\ell)}\right) r^{(\ell)}. \quad (21)$$

Considering initialisation at the fixed point $q^{(1)} = q^*$, such that $q^* = V(q^*)$, gives $q^{(\ell)} = q^*$ for $\ell \geq 1$. These results allow the proof of the following Theorem 2.1.

Theorem 2.1. *Where the recursive relations (19), (20), (21) hold, assuming $0 < V'(q^*) < 1$, $q^{\{1\}(1)} = 0$ and $r^{(1)} = 0$,*

$$\left| \tilde{q}^{\{1\}(\ell)} \right| \leq \frac{\sigma_w^4}{2} \frac{|V''(q^*)| \left| \langle \phi^4(z) \rangle_{q^*} - \langle \phi^2(z) \rangle_{q^*}^2 \right|}{(1 - V'(q^*))^2 (1 + V'(q^*))}, \quad (22)$$

for $\ell \geq 3$.

From Theorem 2.1, and plotting this upper bound in Figure 5, the benefit of increasing q^* for larger sparsity levels is apparent. By stabilising the variance of the hidden layers the next-leading-order correction can be more tightly bounded, and $\tilde{q}^{(\ell)}$ more accurately follows the recursion $q^{(\ell+1)} = V(q^{(\ell)})$ in (4) and (5).

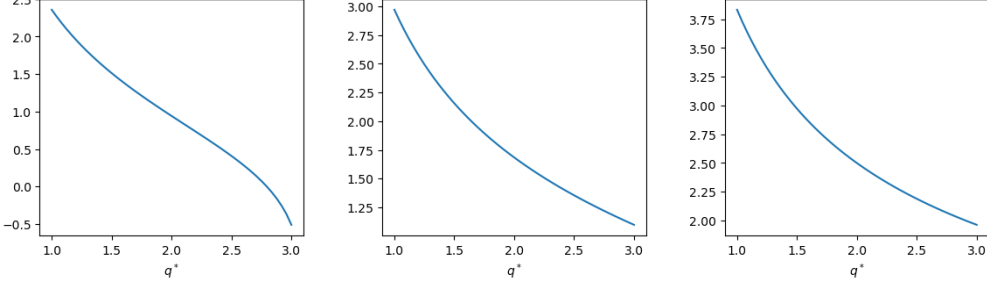


Figure 5: Plots of the log upper bound for the absolute value of the next-leading-order term of the layer variance, $|\tilde{q}^{1\{\ell\}}|$, against q^* , as in (22), for a range of $s = \{0.85, 0.9, 0.95\}$ from left to right, and fixed $m = 2$. By increasing q^* the upper bound for the next-leading-order term $|\tilde{q}^{1\{\ell\}}|$ reduces exponentially.

2.1.3 Sensitivity of $\chi_1^{(\ell)}$

Despite an asymmetry of $V(q)$ around q^* causing a skewed distribution of $\tilde{q}^{(\ell)}$, the explicit reason for an inability to train comes from $\prod_{\ell=1}^L \chi_1(q^{(\ell)})$, therefore the accrued larger values of $\chi_1(q^{(\ell)})$ could instead be reduced by reducing the sensitivity to $q^{(\ell)}$, i.e. reducing $\left| \frac{d\chi_1(q)}{dq} \right|$. The sensitivity of $\chi_1(q)$ to perturbations in q , to the best of our knowledge, has gone undiscussed as a means to regain trainability.

Considering,

$$\chi_{1,\text{CReLU}\tau,m}(q) = \frac{\sigma_w^2}{2} \left[\text{erf}\left(\frac{\tau+m}{\sqrt{2q}}\right) - \text{erf}\left(\frac{\tau}{\sqrt{2q}}\right) \right], \quad (23)$$

note that,

$$\chi'_{1,\text{CReLU}\tau,m}(q) = \frac{\tau\sigma_w^2}{\sqrt{8\pi q^3}} \exp\left(-\frac{(\tau+m)^2}{2q}\right) \left[\exp\left(\frac{2m\tau+\tau^2}{2q}\right) - 1 \right], \quad (24)$$

again full derivations can be found in Section B.

Figure 6 shows that $\chi'_{1,\text{CReLU}\tau,m}(q^*)$ can be reduced at the fixed point q^* by increasing this fixed point, allowing the use of q^* as a parameter to reduce the sensitivity to perturbations of $\chi_{1,\text{CReLU}\tau,m}$ where $\chi'_{1,\text{CReLU}\tau,m}(q^*) > 0$.

2.2 Summary of Findings

Increasing q^* improves the symmetry of the variance map around the fixed point, the fluctuation of the next-leading-order term, and further reduces the sensitivity of $\chi'_{1,\phi}(q^*)$ for our chosen ϕ . In fact, Figures 4, 5 and 6 show that even small increases in q^* to 2 or 3 allow for great improvements across all three considered control metrics. To this endeavor, the largely ignored parameter q^* is shown to be a valuable tool for activations where $V'(q^*)$ approaches 1, especially where dynamical isometry is ruled out by not being approximately linear around the origin.

Particularly for our activation functions, there is an important relationship that appears between $V'_\phi(q)$ and $\chi_{1,\phi}(q)$, found in Price et al. (2024),

$$\chi_{1,\text{CReLU}\tau,m}(q) = V'_{\text{CReLU}\tau,m}(q) + \frac{\sigma_w^2 m}{\sqrt{2\pi q}} \exp\left(-\frac{(\tau+m)^2}{2q}\right). \quad (25)$$

Equation (25) shows the direct relationship between $\chi_{1,\phi}(q)$ and $V'_\phi(q^*)$ for the exemplar choice of $\phi = \text{CReLU}\tau, m$.

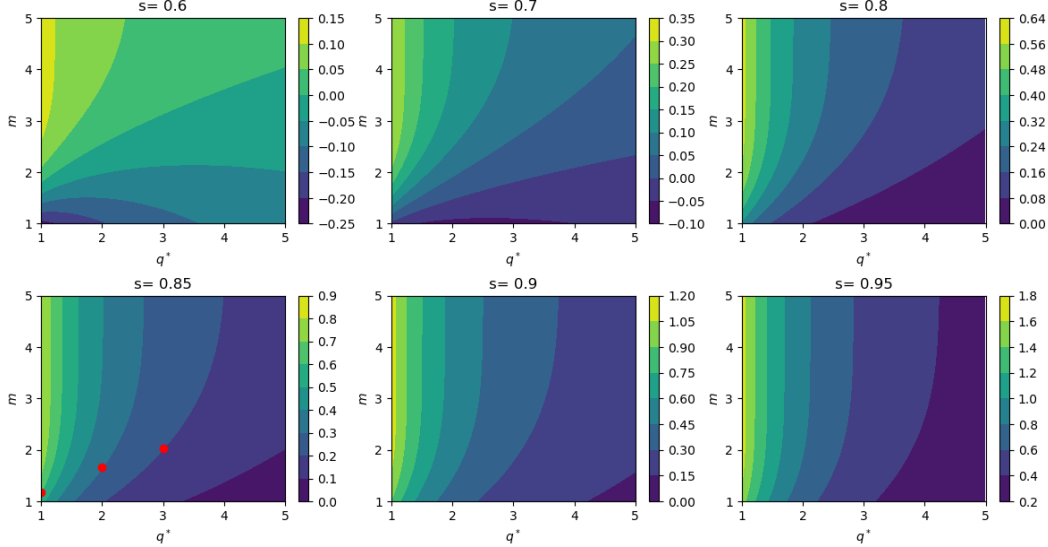


Figure 6: $\chi'_{1,\text{CReLU}_{\tau,m}}(q^*)$, for a range of $s = \{0.6, 0.7, 0.8, 0.85, 0.9, 0.95\}$, the plots of these six sparsities are from left to right then top to bottom, with horizontal axis q^* and vertical axis m . For fixed value m by increasing q^* $\chi'_{1,\text{CReLU}_{\tau,m}}(q^*)$ reduces, and this holds across all six sparsity levels. The highlighted points in plot $s = 0.85$ correspond to fixing $V'(q^*) = 0.7$ for $q^* = \{1, 2, 3\}$.

Then see the relationship between $\chi'_{1,\phi}(q)$ and $V''_\phi(q)$,

$$\chi'_{1,\text{CReLU}_{\tau,m}}(q^*) = V''_{\text{CReLU}_{\tau,m}}(q^*) + \frac{\sigma_w^2 m}{\sqrt{2\pi}q^*} \exp\left(-\frac{(\tau+m)^2}{2q^*}\right) \left(-\frac{1}{2q^*} + \frac{(\tau+m)^2}{2q^{*2}}\right). \quad (26)$$

This relationship shows that by increasing q^* , both $V''_{\text{CReLU}_{\tau,m}}(q^*)$ and $\frac{d\chi_{1,\text{CReLU}_{\tau,m}}}{dq}(q^*)$ can be reduced, Figure 6. Assuming $V''_\phi(q^*) > 0$ is decreasing, this secondary behaviour of the sensitivity reduction of $\chi_{1,\phi}$ should similarly apply to any activation function where you can write $\chi'_{1,\phi}(q) = V''_\phi(q) + f(q)$, given $f(q) > 0$ is decreasing on $q > 0$.

3 Experiments

In order to most clearly demonstrate the need to improve training stability, and the efficacy of our technique, experiments are conducted on DNNs and CNNs of substantial depth and moderate width. The greater depth allows exacerbates the exponential growth of instability while the moderate width retains the stochasticity of the variance, see Sections 2.1.1-2 and 2.1.3 respectively. Specifically, the DNN has depth 100 and width 300 while the CNN has depth 50 and 300 channels per layer; the $\text{CReLU}_{\tau,m}$ nonlinear activation is used in all but the final softmax classification layer. These network hyper parameters are chosen to demonstrate the training capacity between varying q^* rather than maximum achievable accuracy.

Figure 3, 4 and 6, illustrate a substantial difference between their respective quantities for the, somewhat arbitrary, traditional choice of $q^* = 1$ and even modestly larger $q^* = 3$. Throughout this section the nets are initialised with fixed point variances $q^* = \{1, 2, 3\}$ and the training for fixed sparsity s and variance slope $V'(q^*)$ is compared. As the variance slope, $V'(q^*)$, prescribes the first-order behaviour of the variance map, this is a principled quantity to determine the choice of m ; note this is also equivalent to enforcing the probability of falling within the linear region of $\text{CReLU}_{\tau,m}$ due to the relation of $\chi_{1,\text{CReLU}_{\tau,m}}$ and $V'_{\text{CReLU}_{\tau,m}}$ to the normal cdf in (13) and (23). The networks are trained with SGD for 200 and 300 epochs using learning rates 10^{-4} and 10^{-3} for the DNNs and CNNs respectively. The CNNs are also trained with cosine learning rate schedule. SGD is chosen in order that the impact of varying q^* can be isolated as much as possible. The data is split with 20% retained for testing, and 10% of the training data retained for validation, all final results are reported

on the test data set. Each data input is normalized such that it has mean zero and variance q^* , as the first layer has no non-linear activation function applied to it, the initialisation of the first layer is chosen to preserve this. Each experiment is run on a single NVIDIA A100 or H100 for DNNs and CNNs respectively, and implemented in Pytorch Lightning.

Table 1 replicates the results in Price et al. (2023) for $q^* = 1$ and extends the experiments to $q^* = 2$ and 3, as is demonstrated in Figures 4 and 6 this small increase to q^* allows relatively large reduction in $V''(q^*)$ and $\chi'_1(q^*)$. As in Price et al. (2023) sparsity up to 0.8 trains stably for the range of choice of $V'(q^*) = \{0.5, 0.7, 0.9\}$. However, for larger sparsity $s = 0.85$ the network only retains near full accuracy of 91% when $V'(q^*)$ is chosen for more careful associated values of m and for $s = 0.9$ accuracy is reduced and the choice of m becomes more sensitive. Increasing q^* to 2 and 3 both reduces the sensitivity to the choice of m and retains higher accuracy.

Table 2 is analogous to Table 1 but for the CNN where again the experiments of Price et al. (2023) with $q^* = 1$ are shown to have final accuracy with greater sensitivity to $V'(q^*)$; however the median test accuracy is reported rather than the mean, as these tests have greater sensitivity in ability to train. Again, increasing q^* to 2 and 3 generally improves the ability of the nets to train and increases the final accuracy.

The observed sparsity of the trained nets is also shown in Table 1 and Table 2, and is generally consistent with the desired sparsity s . For anomalous cases where a decrease in sparsity is observed these are consistent with occurrences whereby the network fails to train, in these cases where exploding gradients appear the network no longer behaves with hidden layers in line with the expected Gaussian distribution, and hence the reduction in sparsity appears. Though it is worth noting we would generally advocate for somewhat smaller $V'(q^*) = 0.7$ to further control the contraction of $q^{(\ell)}$ towards q^* .

Table 1: DNN trained on MNIST, 100 layers and 300 width, with activation function $\text{CReLU}_{\tau,m}$ across 5 different seeds for each set of parameters. Training was implemented using SGD over 200 epochs with learning rate $\eta = 10^{-4}$ and batch size 64. Results are reported on 20% of data retained for testing.

DNN on MNIST														
			$q^* = 1$				$q^* = 2$				$q^* = 3$			
s	$V'(q^*)$	m	$V''(q^*)$	Accuracy	Sparsity	m	$V''(q^*)$	Accuracy	Sparsity	m	$V''(q^*)$	Accuracy	Sparsity	
ReLU	0.5			0.94	0.50			0.94	0.00			0.94	0.50	
	0.6	0.5	1.22 -0.44	0.91	0.60	1.72 -0.22	0.90	0.60	2.11 -0.15	0.91	0.60			
		0.7	1.63 -0.42	0.90	0.60	2.30 -0.21	0.91	0.60	2.82 -0.14	0.90	0.60			
		0.9	2.25 -0.19	0.92	0.60	3.18 -0.10	0.92	0.60	3.89 -0.06	0.92	0.60			
	0.7	0.5	1.05 -0.37	0.90	0.70	1.49 -0.18	0.90	0.70	1.82 -0.12	0.89	0.70			
		0.7	1.45 -0.31	0.90	0.70	2.05 -0.15	0.90	0.70	2.51 -0.10	0.90	0.70			
		0.9	2.05 -0.04	0.90	0.70	2.90 -0.02	0.91	0.70	3.56 -0.01	0.91	0.70			
	0.8	0.5	0.89 -0.24	0.90	0.80	1.26 -0.12	0.91	0.80	1.54 -0.08	0.91	0.80			
		0.7	1.27 -0.12	0.91	0.80	1.79 -0.06	0.91	0.80	2.19 -0.04	0.90	0.80			
		0.9	1.85 0.21	0.91	0.80	2.62 0.11	0.91	0.80	3.21 0.07	0.91	0.80			
CReLU $_{\tau,m}$	0.8	0.5	0.81 -0.14	0.79	0.85	1.14 -0.07	0.86	0.85	1.40 -0.05	0.90	0.85			
		0.7	1.17 0.02	0.91	0.85	1.66 0.01	0.92	0.85	2.03 0.01	0.91	0.85			
		0.9	1.74 0.41	0.11	0.77	2.46 0.20	0.11	0.76	3.01 0.13	0.27	0.80			
	0.9	0.5	0.72 0.90	0.41	0.90	1.02 0.00	0.49	0.90	1.25 0.00	0.54	0.90			
		0.7	1.06 0.12	0.75	0.90	1.50 0.06	0.61	0.90	1.84 0.04	0.89	0.90			
		0.9	1.61 0.34	0.10	0.84	2.28 0.17	0.11	0.80	2.79 0.11	0.10	0.77			

Figure 7 demonstrates the mean training loss and validation accuracy as a function of gradient descent steps for the DNN at sparsity $s = 0.85$, $V'(q^*) = 0.7$, standard deviation bars are also shown. In all plots the recommended value of $V'(q^*) = 0.7$ is used as it is a value where all networks train. Results for the three representative values of $q = \{1, 2, 3\}$ are displayed. As indicated by the theory in Section 2.1, the training dynamics are generally observed to improve by increasing q^* . Figure 7 shows the training loss and validation accuracy of the DNN for five random seeds. Larger values of q^* typically show substantially faster convergence, while for some seeds less variation is observed. Figures 12-17 in Section E shows plots for individual seeds and for the additional configurations in Table 1; in those plots the importance of larger q^* is shown to become greater as either of sparsity level s and $V'(q^*)$ increase. The improved training speed observed in Figure 7 for greater q^* is apparent, this is in line with the theory in Section 2.1.3 due to the reduction in sensitivity of $\chi_1(q^*)$ for increasing q^* , the corresponding values of $\chi'_1(q^*)$ to the parameter choices in Figures 7 and 8

Table 2: CNN trained on CIFAR10, 50 layers and 300 width, with activation function $\text{CReLU}_{\tau,m}$. Accuracy is the median test accuracy across 4 different seeds. Sparsity is the mean final mean average test sparsity. Training was implemented using SGD over 300 epochs with learning rate $\eta = 10^{-3}$ and cosine learning rate schedule, and batch size 64. Results are reported on 20% of data retained for testing.

CNN on CIFAR10													
		$q^* = 1$				$q^* = 2$				$q^* = 3$			
s	$V'(q^*)$	m	$V''(q^*)$	Accuracy	Sparsity	m	$V''(q^*)$	Accuracy	Sparsity	m	$V''(q^*)$	Accuracy	Sparsity
ReLU	0.5			0.71	0.50			0.75	0.50			0.71	0.50
CReLU $_{\tau,m}$	0.6	0.5	1.22 -0.44	0.70	0.60	1.72 -0.22	0.70	0.60	2.11 -0.15	0.71	0.61		
	0.7	0.5	1.63 -0.42	0.72	0.60	2.30 -0.21	0.72	0.61	2.82 -0.14	0.72	0.60		
	0.9	0.5	2.25 -0.19	0.72	0.60	3.18 -0.10	0.72	0.60	3.89 -0.06	0.73	0.60		
	0.7	0.5	1.05 -0.37	0.65	0.70	1.49 -0.18	0.65	0.71	1.82 -0.12	0.67	0.71		
	0.7	0.5	1.45 -0.31	0.67	0.70	2.05 -0.15	0.68	0.71	2.51 -0.10	0.68	0.71		
	0.9	0.5	2.05 -0.04	0.45	0.71	2.90 -0.02	0.67	0.69	3.56 -0.01	0.63	0.70		
	0.8	0.5	0.89 -0.24	0.57	0.80	1.26 -0.12	0.58	0.80	1.54 -0.08	0.59	0.80		
	0.7	0.5	1.27 -0.12	0.58	0.80	1.79 -0.06	0.60	0.80	2.19 -0.04	0.59	0.80		
	0.9	0.5	1.85 0.21	0.54	0.80	2.62 0.11	0.16	0.81	3.21 0.07	0.28	0.81		
	0.85	0.5	0.81 -0.14	0.51	0.85	1.14 -0.07	0.52	0.85	1.40 -0.05	0.54	0.85		
	0.7	0.5	1.17 0.02	0.49	0.85	1.66 0.01	0.56	0.85	2.03 0.01	0.56	0.85		
	0.9	0.5	1.74 0.41	0.50	0.84	2.46 0.20	0.53	0.84	3.01 0.13	0.51	0.85		
	0.9	0.5	0.72 0.00	0.41	0.90	1.02 0.00	0.43	0.89	1.25 0.00	0.46	0.90		
	0.7	0.5	1.06 0.23	0.29	0.90	0.12 1.50	0.45	0.89	1.84 0.08	0.24	0.90		
	0.9	0.5	1.61 0.69	0.22	0.87	2.28 0.34	0.42	0.88	2.79 0.32	0.35	0.82		

are highlighted as red dots in Figure 6. Figures 18-22 replicates these results for the alternative nonlinear activation $\text{CST}_{\tau,m}$ which suffers from greater training instability.

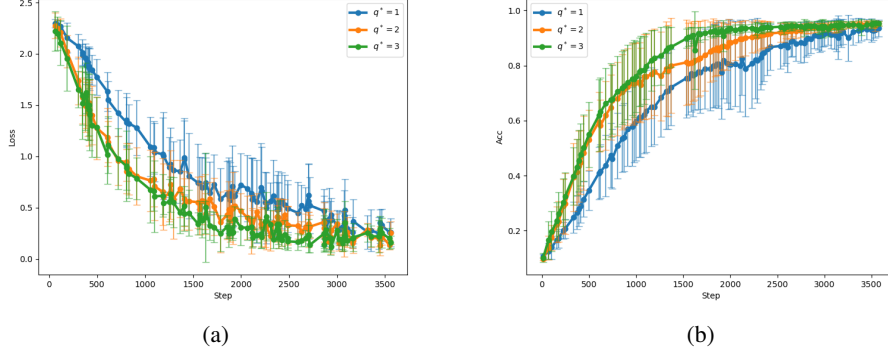


Figure 7: Mean training loss, (a), and validation accuracy, (b), for a DNN trained on MNIST across five seeds, with standard deviation error bars. Trained using SGD with learning rate $\eta = 10^{-4}$ and batch size 64. The DNN is depth 100, width 300 with activation function $\phi = \text{CReLU}_{\tau,m}$. τ and m are chosen such that $s = 0.85$ and $V'(q^*) = 0.7$, across $q^* = \{1, 2, 3\}$. For increasingly larger of $q^* = \{1, 2, 3\}$, the training loss and validation accuracy converge faster.

Figure 8 shows the analogous to Figure 7, mean training loss and validation accuracy as a function of gradient descent steps for the CNN at sparsity $s = 0.85$ and $V'(q^*) = 0.7$ with the three values of $q^* = \{1, 2, 3\}$. The improved training dynamics for greater q^* is again apparent for CNNs, with improved average loss and validation, as well as improved variability in results. Again plots of the training loss for all experiments of the CNNs can be found in Figures 8-27 in Section F.

4 Conclusion and Further Extensions

Previous Edge-of-Chaos analysis has primarily focused on how the correlation of nearby points evolves through the layers of a deep neural network, Poole et al. (2016). For unitary weight matrices and activations that are approximately linear around the origin these correlation dynamics can be improved by having $q^{(\ell)}$ decreasing towards zero; the dynamic isometry property Martens et al. (2021); Roberts & Yaida (2022); Murray et al. (2022). Dynamic isometry isn't possible for activa-

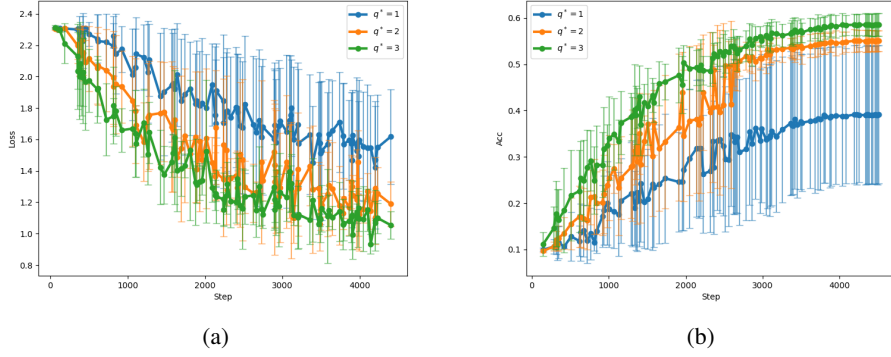


Figure 8: Mean training loss, (a), and mean validation accuracy, (b), against step, for a CNN trained on CIFAR10 across four seeds, with standard deviation error bars. Trained using SGD with cosine learning rate $\eta = 10^{-3}$ and batch size 64. The CNN is depth 50, and has 300 channels with activation function $\phi = \text{CReLU}_{\tau,m}$, τ and m are chosen such that $s = 0.85$ and $V'(q^*) = 0.7$, across $q^* = \{1, 2, 3\}$. For increasingly larger of $q^* = \{1, 2, 3\}$, the training loss and validation accuracy converge faster.

tions that are zero around the origin and new issues of training instability arise Price et al. (2023). This motivates revisiting the role of the Gaussian process variance and showing for the first time that this parameter is a valuable tool for improving the training dynamics of DNNs and CNNs with such sparsifying nonlinear activations. Faster training, less hyper-parameter sensitivity, and greater overall accuracy are obtained for even greater 90% hidden layer sparsities.

This line of research has multiple natural extensions, the most obvious of which are to the more complex architectures such as transformers and state-space models. Both cases include MLP type layers which could similarly benefit from the computational gains suggested by the hidden layer sparsity. Moreover, experiments demonstrating the interplay of our approach with pruned, quantized, and low-rank weight matrices is needed. One can also expect that while $\text{CReLU}_{\tau,m}$ is a particular simple example, that other sparsity inducing activation designs might show further improvements. Lastly, software engineering to demonstrate real world time and energy reductions are needed to encourage the deployment of the theory developed here.

Acknowledgments

The authors would acknowledge support from His Majesty's Government in the development of this research. Jared Tanner is supported by the UK Engineering and Physical Sciences Research Council (EPSRC) through the grant EP/Y028872/1. The authors are also grateful to Thiziri Nait Saada of the University of Oxford for early discussions of this work.

References

Attwell, D. and Laughlin, S. B. An energy budget for signaling in the grey matter of the brain. *Journal of Cerebral Blood Flow and Metabolism: Official Journal of the International Society of Cerebral Blood Flow and Metabolism*, 21(10):1133–1145, October 2001. ISSN 0271-678X. doi: 10.1097/00004647-200110000-00001.

Awasthi, P., Dikkala, N., Kamath, P., and Meka, R. Learning Neural Networks with Sparse Activations. In *Proceedings of Thirty Seventh Conference on Learning Theory*, pp. 406–425. PMLR, June 2024. URL <https://proceedings.mlr.press/v247/awasthi24a.html>.

Blalock, D., Ortiz, J. J. G., Frankle, J., and Guttag, J. What is the State of Neural Network Pruning? In I. Dhillon, D. Papailiopoulos, and V. Sze (eds.), volume 2, pp. 129–146, 2020. URL https://proceedings.mlsys.org/paper_files/paper/2020/file/6c44dc73014d66ba49b28d483a8f8b0d-Paper.pdf.

Bombari, S., Seroussi, I., and Mondelli, M. Better Rates for Private Linear Regression in the Proportional Regime via Aggressive Clipping. In *High-dimensional Learning Dynamics 2025*, June 2025. URL <https://openreview.net/forum?id=UUgXMJW7iB>.

Chizat, L., Oyallon, E., and Bach, F. On Lazy Training in Differentiable Programming. In *Advances in Neural Information Processing Systems*, volume 32. Curran Associates, Inc., 2019. URL https://proceedings.neurips.cc/paper_files/paper/2019/hash/ae614c557843b1df326cb29c57225459-Abstract.html.

Dominé, C. C., Braun, L., Fitzgerald, J. E., and Saxe, A. M. Exact learning dynamics of deep linear networks with prior knowledge^{*}. *Journal of Statistical Mechanics: Theory and Experiment*, 2023(11):114004, November 2023. ISSN 1742-5468. doi: 10.1088/1742-5468/ad01b8. URL <https://iopscience.iop.org/article/10.1088/1742-5468/ad01b8>.

Dominé, C. C. J., Anguita, N., Proca, A. M., Braun, L., Kunin, D., Mediano, P. A. M., and Saxe, A. M. From Lazy to Rich: Exact Learning Dynamics in Deep Linear Networks. In *The Thirteenth International Conference on Learning Representations*, October 2024. URL <https://openreview.net/forum?id=ZXaocmXc6d>.

Frankle, J. and Carbin, M. The Lottery Ticket Hypothesis: Finding Sparse, Trainable Neural Networks. In *International Conference on Learning Representations*, September 2018. URL <https://openreview.net/forum?id=rJ1-b3RcF7>.

Hanin, B. Random neural networks in the infinite width limit as Gaussian processes. *The Annals of Applied Probability*, 33(6A), December 2023. ISSN 1050-5164. doi: 10.1214/23-AAP1933. URL <https://projecteuclid.org/journals/annals-of-applied-probability/volume-33/issue-6A/Random-neural-networks-in-the-infinite-width-limit-as-Gaussian/10.1214/23-AAP1933.full>.

Howard, A. G., Zhu, M., Chen, B., Kalenichenko, D., Wang, W., Weyand, T., Andreetto, M., and Adam, H. MobileNets: Efficient Convolutional Neural Networks for Mobile Vision Applications, April 2017. URL <https://arxiv.org/abs/1704.04861>. arXiv:1704.04861 [cs].

Hu, E. J., Shen, Y., Wallis, P., Allen-Zhu, Z., Li, Y., Wang, S., Wang, L., and Chen, W. LoRA: Low-Rank Adaptation of Large Language Models, October 2021. URL <https://arxiv.org/abs/2106.09685>. arXiv:2106.09685 [cs].

Lee, J., Bahri, Y., Novak, R., Schoenholz, S. S., Pennington, J., and Sohl-Dickstein, J. Deep Neural Networks as Gaussian Processes. In *International Conference on Learning Representations*, February 2018. URL <https://openreview.net/forum?id=B1EA-M-0Z>.

Luo, Y., Song, C., Han, X., Chen, Y., Xiao, C., Meng, X., Deng, L., Wei, J., Liu, Z., and Sun, M. Sparsing Law: Towards Large Language Models with Greater Activation Sparsity. In *Proceedings of the 42nd International Conference on Machine Learning*, pp. 41311–41330. PMLR, October 2025. URL <https://proceedings.mlr.press/v267/luo25i.html>.

Mai, V. V. and Johansson, M. Stability and Convergence of Stochastic Gradient Clipping: Beyond Lipschitz Continuity and Smoothness. In *Proceedings of the 38th International Conference on Machine Learning*, pp. 7325–7335. PMLR, July 2021. URL <https://proceedings.mlr.press/v139/mai21a.html>.

Marshall, N., Xiao, K. L., Agarwala, A., and Paquette, E. To Clip or not to Clip: the Dynamics of SGD with Gradient Clipping in High-Dimensions. In *The Thirteenth International Conference on Learning Representations*, October 2024. URL <https://openreview.net/forum?id=jmN1zXMq00>.

Martens, J., Ballard, A., Desjardins, G., Swirszcz, G., Dalibard, V., Sohl-Dickstein, J., and Schoenholz, S. S. Rapid training of deep neural networks without skip connections or normalization layers using Deep Kernel Shaping, October 2021. URL <http://arxiv.org/abs/2110.01765> [cs]. arXiv:2110.01765 [cs].

Matthews, A. G. d. G., Hron, J., Rowland, M., Turner, R. E., and Ghahramani, Z. Gaussian Process Behaviour in Wide Deep Neural Networks. In *International Conference on Learning Representations*, February 2018. URL <https://openreview.net/forum?id=H1-nGgWC->.

Menghani, G. Efficient Deep Learning: A Survey on Making Deep Learning Models Smaller, Faster, and Better. *ACM Comput. Surv.*, 55(12):259:1–259:37, March 2023. ISSN 0360-0300. doi: 10.1145/3578938. URL <https://dl.acm.org/doi/10.1145/3578938>.

Murray, M., Abrol, V., and Tanner, J. Activation function design for deep networks: linearity and effective initialisation. *Applied and Computational Harmonic Analysis*, 59:117–154, July 2022. ISSN 1063-5203. doi: 10.1016/j.acha.2021.12.010. URL <https://www.sciencedirect.com/science/article/pii/S1063520320321001111>.

Muthukumar, R. and Sulam, J. Sparsity-aware generalization theory for deep neural networks. In *Proceedings of Thirty Sixth Conference on Learning Theory*, pp. 5311–5342. PMLR, July 2023. URL <https://proceedings.mlr.press/v195/muthukumar23a.html>.

Neal, R. M. *Bayesian Learning for Neural Networks*, volume 118 of *Lecture Notes in Statistics*. Springer, New York, NY, 1996. ISBN 978-0-387-94724-2 978-1-4612-0745-0. doi: 10.1007/978-1-4612-0745-0. URL <http://link.springer.com/10.1007/978-1-4612-0745-0>.

Osawa, K., Sekiya, A., Naganuma, H., and Yokota, R. Accelerating Matrix Multiplication in Deep Learning by Using Low-Rank Approximation. In *2017 International Conference on High Performance Computing & Simulation (HPCS)*, pp. 186–192, July 2017. doi: 10.1109/HPCS.2017.37. URL <https://ieeexplore.ieee.org/document/8035076>.

Pascanu, R., Mikolov, T., and Bengio, Y. On the difficulty of training recurrent neural networks. In *Proceedings of the 30th International Conference on Machine Learning*, pp. 1310–1318. PMLR, May 2013. URL <https://proceedings.mlr.press/v28/pascanu13.html>.

Pennington, J., Schoenholz, S., and Ganguli, S. Resurrecting the sigmoid in deep learning through dynamical isometry: theory and practice. In *Advances in Neural Information Processing Systems*, volume 30. Curran Associates, Inc., 2017. URL https://proceedings.neurips.cc/paper_files/paper/2017/hash/d9fc0cdb67638d50f411432d0d41d0ba-Abstract.html.

Pennington, J., Schoenholz, S., and Ganguli, S. The emergence of spectral universality in deep networks. In *Proceedings of the Twenty-First International Conference on Artificial Intelligence and Statistics*, pp. 1924–1932. PMLR, March 2018. URL <https://proceedings.mlr.press/v84/pennington18a.html>.

Poole, B., Lahiri, S., Raghu, M., Sohl-Dickstein, J., and Ganguli, S. Exponential expressivity in deep neural networks through transient chaos. In *Advances in Neural Information Processing Systems*, volume 29. Curran Associates, Inc., 2016. URL https://papers.nips.cc/paper_files/paper/2016/hash/148510031349642de5ca0c544f31b2ef-Abstract.html.

Price, I., Ball, N. D., Jones, A. C., Lam, S. C. H., and Tanner, J. DEEP NEURAL NETWORK INITIALIZATION WITH SPARSITY INDUCING ACTIVATIONS. In *The Twelfth International Conference on Learning Representations*, October 2023. URL <https://openreview.net/forum?id=uvXK8Xk9Jk>.

Price, I., Ball, N. D., Lam, S. C. H., Jones, A. C., and Tanner, J. Deep Neural Network Initialization with Sparsity Inducing Activations, February 2024. URL <http://arxiv.org/abs/2402.16184> arXiv: 2402.16184 [cs].

Roberts, D. A. and Yaida, S. *The Principles of Deep Learning Theory: An Effective Theory Approach to Understanding Neural Networks*. Cambridge University Press, Cambridge, 2022. ISBN 978-1-316-51933-2. doi: 10.1017/9781009023405. URL <https://www.cambridge.org/core/books/principles-of-deep-learning-theory/3E566F65026D6896DC814A8C31EF3B4C>.

Schoenholz, S. S., Gilmer, J., Ganguli, S., and Sohl-Dickstein, J. Deep Information Propagation. In *International Conference on Learning Representations*, February 2017. URL <https://openreview.net/forum?id=H1W1UN9gg>.

Weng, O. Neural Network Quantization for Efficient Inference: A Survey, January 2023. URL <http://arxiv.org/abs/2112.06126>. arXiv:2112.06126 [cs].

Xiao, L., Bahri, Y., Sohl-Dickstein, J., Schoenholz, S., and Pennington, J. Dynamical Isometry and a Mean Field Theory of CNNs: How to Train 10,000-Layer Vanilla Convolutional Neural Networks. In *Proceedings of the 35th International Conference on Machine Learning*, pp. 5393–5402. PMLR, July 2018. URL <https://proceedings.mlr.press/v80/xiao18a.html>.

Xie, Y., Mihalas, S., and Kuśmierz, L. Slow Transition to Low-Dimensional Chaos in Heavy-Tailed Recurrent Neural Networks, October 2025. URL <http://arxiv.org/abs/2505.09816> arXiv:2505.09816 [q-bio].

Yaida, S. Non-Gaussian processes and neural networks at finite widths. In *Proceedings of The First Mathematical and Scientific Machine Learning Conference*, pp. 165–192. PMLR, August 2020. URL <https://proceedings.mlr.press/v107/yaida20a.html>.

Yang, G. and Schoenholz, S. Mean Field Residual Networks: On the Edge of Chaos. In *Advances in Neural Information Processing Systems*, volume 30. Curran Associates, Inc., 2017. URL https://proceedings.neurips.cc/paper_files/paper/2017/hash/81c650caac28cdefce4de5ddc18befa0-Abstract.html.

You, C., Wu, K., Jia, Z., Chen, L., Bhojanapalli, S., Guo, J., Evci, U., Wassenberg, J., Netrapalli, P., Willcock, J. J., Subramanian, S., Chern, F., Andreev, A., Pathak, S., Yu, F. X., Jain, P., Culler, D. E., Levy, H., and Kumar, S. Spark Transformer: Reactivating Sparsity in Transformer FFN and Attention. In *The Thirty-ninth Annual Conference on Neural Information Processing Systems*, October 2025. URL <https://openreview.net/forum?id=o4zN34ahEK>.

Zhang, J., He, T., Sra, S., and Jadbabaie, A. Why Gradient Clipping Accelerates Training: A Theoretical Justification for Adaptivity. In *International Conference on Learning Representations*, September 2019. URL <https://openreview.net/forum?id=BJgnXpVYwS>.

Zhang, Z., Song, Y., Yu, G., Han, X., Lin, Y., Xiao, C., Song, C., Liu, Z., Mi, Z., and Sun, M. ReLU² Wins: Discovering Efficient Activation Functions for Sparse LLMs, February 2024. URL <http://arxiv.org/abs/2402.03804>. arXiv:2402.03804 [cs].

A Further on χ_1

To further understand the importance of χ_1 consider, as in Xiao et al. (2018), the input-output Jacobian,

$$J = \frac{\partial x^{(L)}}{\partial x^{(0)}} = \prod_{l=1}^L D^l W^l. \quad (27)$$

The Jacobian is the product of the linear operators used in computing each layer's error vector in backpropagation, and therefore is closely related to training.

Assuming a normalized input so that $q^{(1)} = q^*$, the moments of $D^{(\ell)}$ are given by,

$$\mu_k = \int (\phi'(\sqrt{q^*}z))^{2k} \gamma(dz). \quad (28)$$

(Note: $\sigma_w^2 \mu_1 = \chi_1$) The quantities μ_1, μ_2 are then related to the first two moments of the spectrum of JJ^T, m_1, m_2 , by the following,

$$m_1 = (\sigma_w^2 \mu_1)^L, \quad (29)$$

$$m_2 = (\sigma_w^2 \mu_1)^{2L} L \left(\frac{\mu_2}{\mu_1^2} + \frac{1}{L} - 1 - s_1 \right), \quad (30)$$

where s_1 is the first moment of WW^T S -transformed, and so we have identified $m_1 = (\chi_1)^L$. For our case of initialisation, W is Gaussian with mean 0 and variance $\sigma_w^2/N_{\ell-1}$, $s_1 = -1$.

Since $m_1 = (\chi_1)^L$, we can interpret χ_1 as the growth of the error vector per layer. The motivation of concentrating χ_1 around 1 is therefore to ensure for large L the growth of the error vectors doesn't explode or collapse in expectation.

To further stabilize our network, we can concentrate the variance of JJ^T ,

$$\sigma_{JJ^T} = m_2 - m_1^2 = L \left(\frac{\mu_2}{\mu_1^2} - 1 - s_1 \right). \quad (31)$$

As the variance $\sigma_{JJ^T}^2$ increases with depth L this may become problematic for large depth. Methods have been proposed to control $\sigma_{JJ^T}^2$, for example in Pennington et al. (2018) they proposed allowing $q^* \rightarrow 0$ at a rate to ensure σ_{JJ^T} converges to a nonzero constant in the large depth limit. Further studies show in the case of $\phi = \text{ReLU}$, there is only one EoC point and so σ_{JJ^T} is fixed with no way to improve it Pennington et al. (2018). If instead $\phi(\cdot)$ is approximately linear around the origin, with orthonormal activations then $s_1 = 0$, and it is possible to have $\frac{\mu_2}{\mu_1^2} \geq 1$ approach 1 in order to mitigate the growth of σ_{JJ^T} Murray et al. (2022), such as $\frac{\mu_2}{\mu_1^2} \sim L^{-1}$ Martens et al. (2021).

In our case, for $\phi(\cdot)$ where $\phi(z) = 0$ with $|z| \leq \tau$, no such L independence is possible; however $\frac{\mu_2}{\mu_1^2} - 1 - s_1$ remains a function of m, τ, q^* .

B Derivation of Further Derivatives for CReLU $_{\tau,m}$ and CST $_{\tau,m}$

We know,

$$V'_{\text{CReLU}_{\tau,m}}(q) = \sigma_w^2 \left(\frac{1}{2} \text{erf} \left(\frac{\tau + m}{\sqrt{2q}} \right) - \frac{1}{2} \text{erf} \left(\frac{\tau}{\sqrt{2q}} \right) - \frac{m}{\sqrt{2\pi q}} \exp \left(-\frac{(\tau + m)^2}{2q} \right) \right) \quad (32)$$

$$= \sigma_w^2 (a_1 + a_2 + a_3), \quad (33)$$

which we write as,

$$V'_{\text{CReLU}_{\tau,m}}(q) = \sigma_w^2 (a_1 + a_2 + a_3), \quad (34)$$

defining,

$$a_1 = \frac{1}{2} \operatorname{erf} \left(\frac{\tau + m}{\sqrt{2q}} \right), \quad (35)$$

$$a_2 = -\frac{1}{2} \operatorname{erf} \left(\frac{\tau}{\sqrt{2q}} \right), \quad (36)$$

$$a_3 = -\frac{m}{\sqrt{2\pi}q} \exp \left(-\frac{(\tau + m)^2}{2q} \right). \quad (37)$$

It follows that,

$$\frac{da_1}{dq} = -\frac{\tau + m}{\sqrt{8\pi}q^3} e^{-\left(\frac{\tau+m}{\sqrt{2q}}\right)^2}, \quad (38)$$

$$\frac{da_2}{dq} = \frac{\tau}{\sqrt{8\pi}q^3} e^{-\left(\frac{\tau}{\sqrt{2q}}\right)^2}, \quad (39)$$

$$\frac{da_3}{dq} = \frac{m}{\sqrt{8\pi}q^3} \left(1 - \frac{(\tau + m)^2}{q} \right) \exp \left(-\frac{(\tau + m)^2}{2q} \right). \quad (40)$$

Hence,

$$V''_{\text{CReLU}_{\tau,m}}(q) = \frac{\sigma_w^2}{\sqrt{8\pi}q^3} \left(\tau e^{-\left(\frac{\tau}{\sqrt{2q}}\right)^2} - (\tau + m) e^{-\left(\frac{\tau+m}{\sqrt{2q}}\right)^2} + m \left(1 - \frac{(\tau + m)^2}{q} \right) \exp \left(-\frac{(\tau + m)^2}{2q} \right) \right). \quad (41)$$

Now since $V'_{\text{CST}_{\tau,m}}(q) = 2V'_{\text{CReLU}_{\tau,m}}(q)$, $V''_{\text{CST}_{\tau,m}}(q) = 2V''_{\text{CReLU}_{\tau,m}}(q)$.

Further, we can calculate $\chi'_{1,\text{CReLU}_{\tau,m}}$ and $\chi'_{1,\text{CST}_{\tau,m}}$ since, $\chi_{1,\text{CReLU}_{\tau,m}} = \sigma_w^2(a_1 + a_2)$, we can immediately see,

$$\chi'_{1,\text{CReLU}_{\tau,m}} = \frac{\sigma_w^2}{\sqrt{8\pi}q^3} \left(\tau e^{-\left(\frac{\tau}{\sqrt{2q}}\right)^2} - (\tau + m) e^{-\left(\frac{\tau+m}{\sqrt{2q}}\right)^2} \right). \quad (42)$$

Again $\chi'_{1,\text{CST}_{\tau,m}} = 2\chi'_{1,\text{CReLU}_{\tau,m}}$, so

$$\chi_{1,\text{CST}_{\tau,m}}(q) = V'_{\text{CST}_{\tau,m}}(q) + \frac{\sqrt{2}\sigma_w^2 m}{\sqrt{\pi}q} \exp \left(-\frac{(\tau + m)^2}{2q} \right). \quad (43)$$

C Variance Map Analysis for $\text{CST}_{\tau,m}$

It was shown in Price et al. (2024) that

$$V'_{\text{CST}_{\tau,m}}(q) = 2V'_{\text{CReLU}_{\tau,m}}(q), \quad (44)$$

and

$$\chi'_{1,\text{CST}_{\tau,m}}(q) = 2\chi'_{1,\text{CReLU}_{\tau,m}}(q). \quad (45)$$

Therefore the derivatives of the variance map for $\text{CST}_{\tau,m}$, and derivatives of $\chi_{1,\text{CST}_{\tau,m}}$ are equivalent to $\text{CReLU}_{\tau,m}$ up to a factor of 2. Plots of $V'_{\text{CST}_{\tau,m}}(q^*)$, $V''_{\text{CST}_{\tau,m}}(q^*)$ and $\chi'_{1,\text{CST}_{\tau,m}}(q^*)$ can be found in Figures 9, 10 and 11, respectively.

Figures 9, 10, 11 show that we can, similarly to $\text{CReLU}_{\tau,m}$, decrease the values $V'_{\text{CST}_{\tau,m}}(q^*)$, $V''_{\text{CST}_{\tau,m}}(q^*)$ and $\chi'_{1,\text{CST}_{\tau,m}}(q^*)$ for fixed m by increasing q^* .

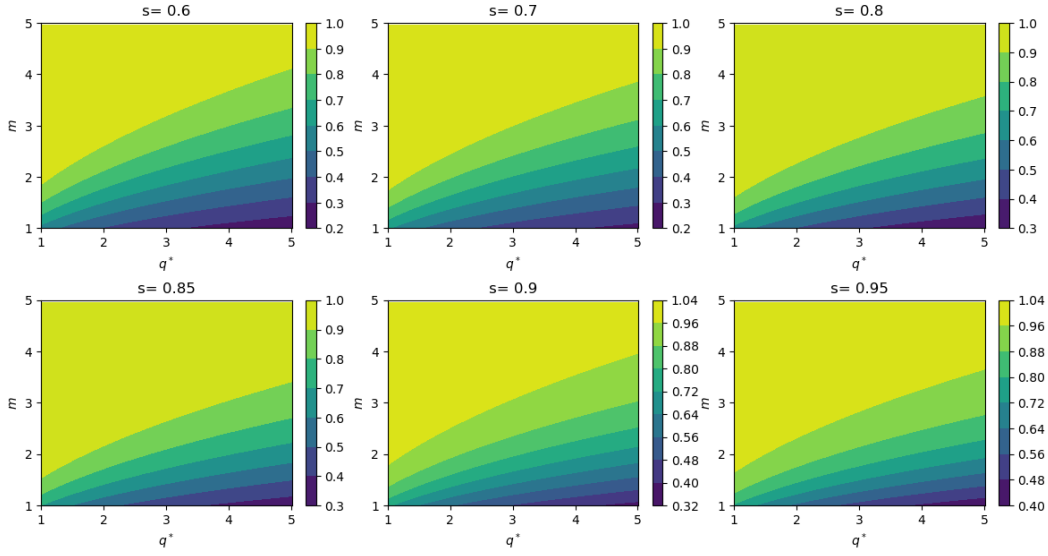


Figure 9: $V'_{CST_{\tau,m}}(q^*)$ for a range of $s = \{0.6, 0.7, 0.8, 0.85, 0.9, 0.95\}$, the plots of these six sparsities are from left to right then top to bottom, with horizontal axis q^* and vertical axis m . For fixed value m by increasing q^* , $V'_{CST_{\tau,m}}(q)$ reduces, and this holds across all six sparsity levels.

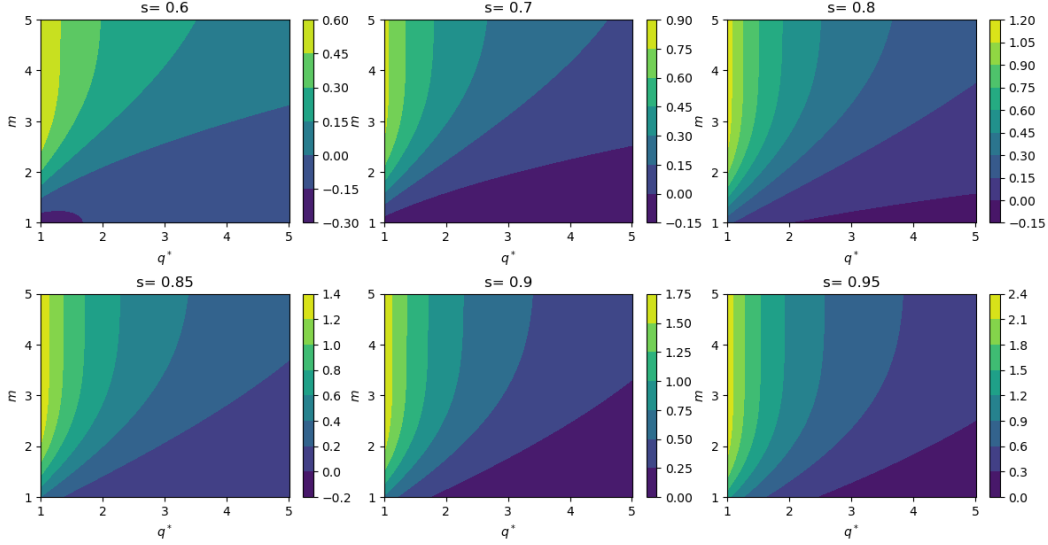


Figure 10: $V''_{CST_{\tau,m}}(q^*)$, for a range of $s = \{0.6, 0.7, 0.8, 0.85, 0.9, 0.95\}$, the plots of these six sparsities are from left to right then top to bottom, with horizontal axis q^* and vertical axis m . For high sparsity levels $s = \{0.7, 0.8, 0.85, 0.9, 0.95\}$, and large fixed value m by increasing q^* , $V''_{CST_{\tau,m}}(q^*)$ reduces.

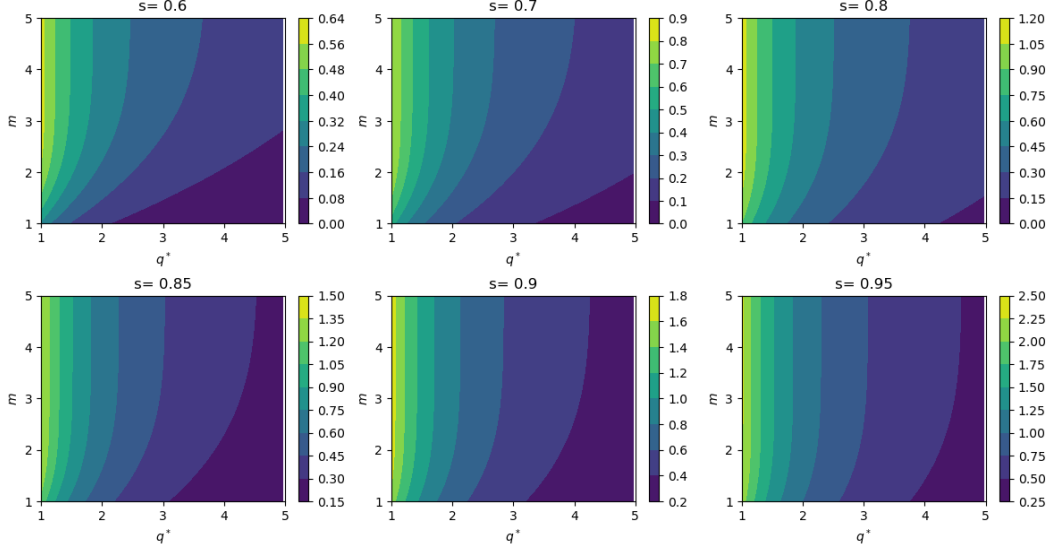


Figure 11: $\chi'_{1,CST_{\tau,m}}(q^*)$, for a range of $s = \{0.6, 0.7, 0.8, 0.85, 0.9, 0.95\}$, the plots of these six sparsities are from left to right then top to bottom, with horizontal axis q^* and vertical axis m . For fixed value m by increasing q^* , $\chi'_{1,CST_{\tau,m}}(q^*)$ reduces, and this holds across all six sparsity levels.

D Finite Dimensional Correction

To show the precise appearance of the second derivative in the finite dimensional correction we can look to the work of Chapters 4 and 5, Roberts & Yaida (2022), they find the following equivalent recursions,

$$q^{(\ell+1)} = V(q^{(\ell)}) \quad (46)$$

$$r^{(\ell+1)} = \left(V'(q^{(\ell)}) \right)^2 r^{(\ell)} + \sigma_w^4 \left(\langle \phi^4(z) \rangle_{q^{(\ell)}} - \langle \phi^2(z) \rangle_{q^{(\ell)}}^2 \right) \quad (47)$$

$$\tilde{q}^{(1)(\ell+1)} = V'(q^{(\ell)}) \tilde{q}^{(1)(\ell)} + \frac{1}{2} V''(q^{(\ell)}) r^{(\ell)}. \quad (48)$$

We know from Roberts & Yaida (2022) that the first-layer pre-activation distribution is exactly Gaussian, hence $\tilde{q}^{(1)(1)} = 0$ and $r^{(1)} = 0$. Since we initialise at the fixed point $q^{(1)} = q^*$, such that $q^* = V(q^*)$, immediately $q^{(\ell)} = q^*$ for $\ell \geq 1$.

The following Theorem D.1, Theorem D.2 will prove useful.

Lemma D.1. *Where the following recursive relation holds,*

$$r^{(\ell+1)} = V'(q^*)^2 r^{(\ell)} + \sigma_w^4 \left(\langle \phi^4(z) \rangle_{q^*} - \langle \phi^2(z) \rangle_{q^*}^2 \right), \quad (49)$$

assuming $V'(q^*) \neq 1$ and $r^{(1)} = 0$,

$$r^{(\ell)} = \sigma_w^4 \left(\langle \phi^4(z) \rangle_{q^*} - \langle \phi^2(z) \rangle_{q^*}^2 \right) \frac{1 - V'(q^*)^{2(\ell-1)}}{1 - V'(q^*)^2}, \quad (50)$$

for $\ell \geq 2$.

Proof. We have a recursive formula for $r^{(\ell)}$ of the form $r^{(\ell+1)} = ar^{(\ell)} + b$, where $a = V'(q^*)^2$ and $b = \sigma_w^4 \left(\langle \phi^4(z) \rangle_{q^*} - \langle \phi^2(z) \rangle_{q^*}^2 \right)$, hence for $\ell \geq 2$,

$$r^{(\ell)} = \sigma_w^4 \left(\langle \phi^4(z) \rangle_{q^*} - \langle \phi^2(z) \rangle_{q^*}^2 \right) \sum_{0 \leq i \leq \ell-2} V'(q^*)^{2i}. \quad (51)$$

Since $V'(q^*) \neq 1$, we can simply apply the geometric series formula to find the result,

$$r^{(\ell)} = \sigma_w^4 \left(\langle \phi^4(z) \rangle_{q^*} - \langle \phi^2(z) \rangle_{q^*}^2 \right) \frac{1 - V'(q^*)^{2(\ell-1)}}{1 - V'(q^*)^2}. \quad (52)$$

□

Lemma D.2. *Where the following recursive relationship holds,*

$$\tilde{q}^{\{1\}(\ell+1)} = V'(q^*) \tilde{q}^{\{1\}(\ell)} + \frac{1}{2} V''(q^*) r^{(\ell)}, \quad (53)$$

and we initialise such that $\tilde{q}^{\{1\}(1)} = 0$ and $r^{(1)} = 0$, then

$$\tilde{q}^{\{1\}(\ell)} = \frac{1}{2} V''(q^*) \sum_{0 \leq i \leq \ell-3} V'(q^*)^i r^{(\ell-i-1)}, \quad (54)$$

for $\ell \geq 3$.

Proof. We prove this result by induction. To begin, we identify $\tilde{q}^{\{1\}(2)} = V'(q^*) \tilde{q}^{\{1\}(1)} + \frac{1}{2} V''(q^*) r^{(1)} = 0$. Now for $\ell = 3$,

$$\tilde{q}^{\{1\}(3)} = V'(q^*) \tilde{q}^{\{1\}(2)} + \frac{1}{2} V''(q^*) r^{(2)} = \frac{1}{2} V''(q^*) r^{(2)}. \quad (55)$$

Let us then assume the result holds for $\ell = n$ so,

$$\tilde{q}^{\{1\}(n)} = \frac{1}{2} V''(q^*) \sum_{0 \leq i \leq n-3} V'(q^*)^i r^{(n-i-1)}. \quad (56)$$

Hence for $\ell = n + 1$,

$$\tilde{q}^{\{1\}(n+1)} = V'(q^*) \tilde{q}^{\{1\}(n)} + \frac{1}{2} V''(q^*) r^{(n)} \quad (57)$$

$$= V'(q^*) \frac{1}{2} V''(q^*) \sum_{0 \leq i \leq n-3} V'(q^*)^i r^{(n-i-1)} + \frac{1}{2} V''(q^*) r^{(n)} \quad (58)$$

$$= \frac{1}{2} V''(q^*) \sum_{0 \leq i \leq n-2} V'(q^*)^i r^{(n-i)}, \quad (59)$$

as required. This completes our proof. □

Proof of Theorem 2.1. We can substitute our equation for $r^{(\ell)}$ from Theorem D.1 into our result for $\tilde{q}^{\{1\}(\ell)}$ found in Theorem D.2. Since $V'(q^*) \neq 1$, for $\ell \geq 3$

$$\tilde{q}^{\{1\}(\ell)} = \frac{\sigma_w^4}{2} V''(q^*) \left(\langle \phi^4(z) \rangle_{q^*} - \langle \phi^2(z) \rangle_{q^*}^2 \right) \sum_{0 \leq i \leq \ell-3} V'(q^*)^i \frac{1 - V'(q^*)^{2(\ell-i-1)}}{1 - V'(q^*)^2} \quad (60)$$

$$= \frac{\sigma_w^4}{2} \frac{V''(q^*)}{1 - V'(q^*)^2} \left(\langle \phi^4(z) \rangle_{q^*} - \langle \phi^2(z) \rangle_{q^*}^2 \right) \sum_{0 \leq i \leq \ell-3} V'(q^*)^i - V'(q^*)^{2\ell-i-2} \quad (61)$$

$$= \frac{\sigma_w^4}{2} \frac{V''(q^*)}{1 - V'(q^*)^2} \left(\langle \phi^4(z) \rangle_{q^*} - \langle \phi^2(z) \rangle_{q^*}^2 \right) \times \left[\frac{1 - V'(q^*)^{\ell-2}}{1 - V'(q^*)} - V'(q^*)^{2\ell-2} \frac{1 - V'(q^*)^{2-\ell}}{1 - V'(q^*)^{-1}} \right] \quad (62)$$

$$= \frac{\sigma_w^4}{2} \frac{V''(q^*)}{1 - V'(q^*)^2} \left(\langle \phi^4(z) \rangle_{q^*} - \langle \phi^2(z) \rangle_{q^*}^2 \right) \times \left[\frac{1 - V'(q^*)^{\ell-2} + V'(q^*)^{2\ell-1} - V'(q^*)^{\ell+1}}{1 - V'(q^*)} \right] \quad (63)$$

$$= \frac{\sigma_w^4}{2} \frac{V''(q^*)}{1 - V'(q^*)^2} \left(\langle \phi^4(z) \rangle_{q^*} - \langle \phi^2(z) \rangle_{q^*}^2 \right) \times \left[\frac{(1 - V'(q^*)^{\ell-2})(1 - V'(q^*)^{\ell+1})}{1 - V'(q^*)} \right]. \quad (64)$$

Further, considering our assumption $0 < V'(q^*) < 1$ and taking the absolute value, we find,

$$\left| \tilde{q}^{\{1\}(\ell)} \right| \leq \frac{\sigma_w^4}{2} \frac{|V''(q^*)|}{(1 - V'(q^*))^2 (1 + V'(q^*))} \left| \langle \phi^4(z) \rangle_{q^*} - \langle \phi^2(z) \rangle_{q^*}^2 \right|, \quad (65)$$

for $\ell \geq 3$. This completes our proof. \square

E Further DNN Experiment Results

This section provides more figures for the training loss behaviour of DNNs when increasing q^* for exemplar activation functions $\text{CReLU}_{\tau,m}$ and $\text{CST}_{\tau,m}$; further detail of experiments in Section 3.

E.1 CReLU $_{\tau,m}$

E.1.1 Mean Training Loss Plots

Figure 12 provides the mean training loss for each individual run, and demonstrates the improvement in mean training dynamics, with faster training for high sparsity levels, particularly for cases $s = \{0.85, 0.9\}$, $V'(q^*) = \{0.5, 0.7\}$; and the recovery of ability to train for $s = 0.85$, $V'(q^*) = 0.9$.

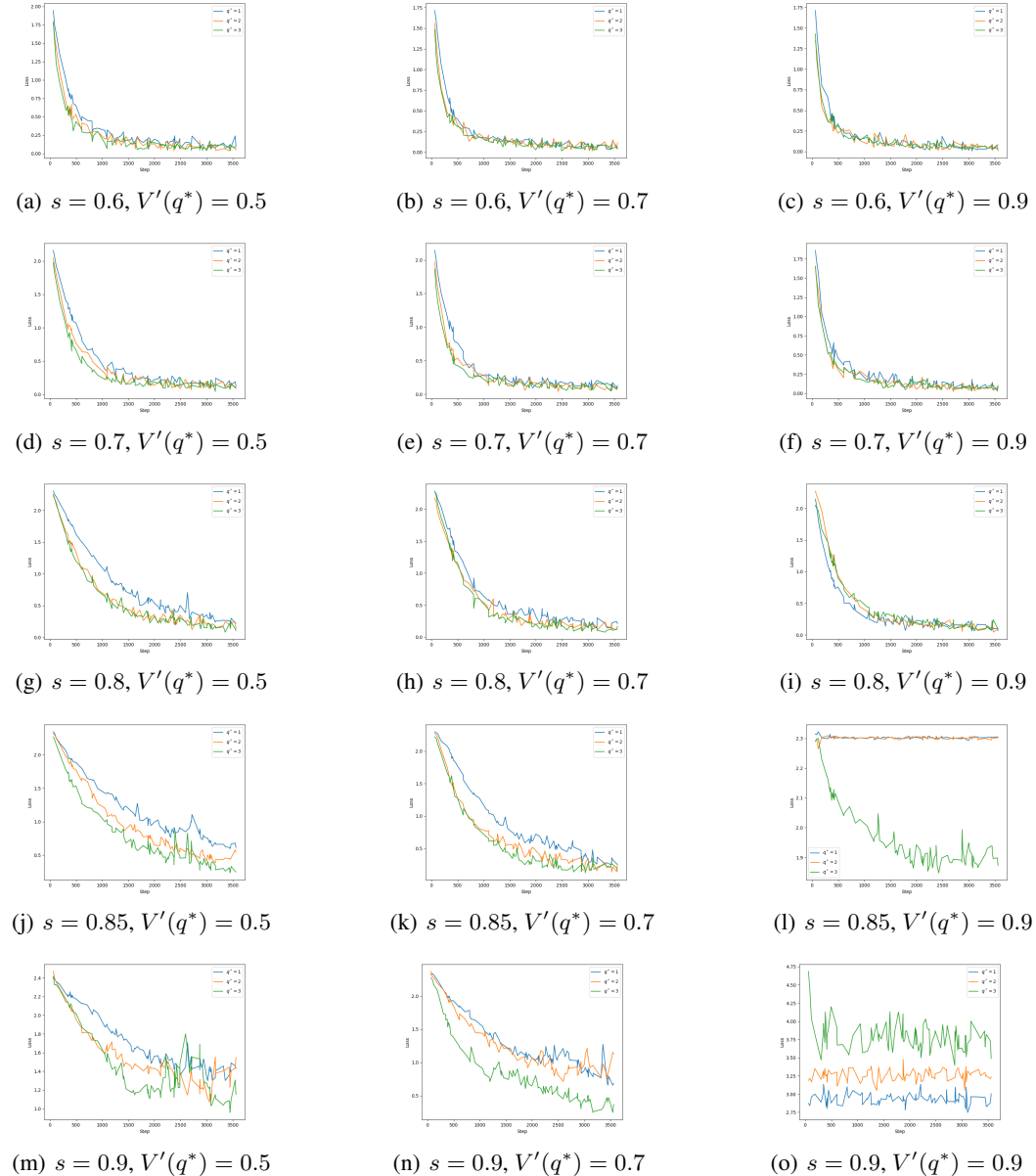


Figure 12: Mean training loss across five seeds for a DNN depth 100 and width 300, trained on MNIST, batch size 64 and learning rate $\eta = 10^{-4}$, for activation function $\phi = \text{CReLU}_{\tau,m}$, with τ and m chosen such that $s, V'(q^*)$ are as described.

E.1.2 Individual Run Training Loss Plots

Now for a better look at each individual test, and clearer analysis of when recovery to train is found see the Figures 13-17, which demonstrate the individual run improvement in training speed with increased q^* for DNNs of depth 100 and width 300 trained on MNIST with activation $\text{CReLU}_{\tau,m}$, as well as a recovery in ability to train for $s = 0.85$, $V'(q^*) = 0.9$ when $q^* = 3$.

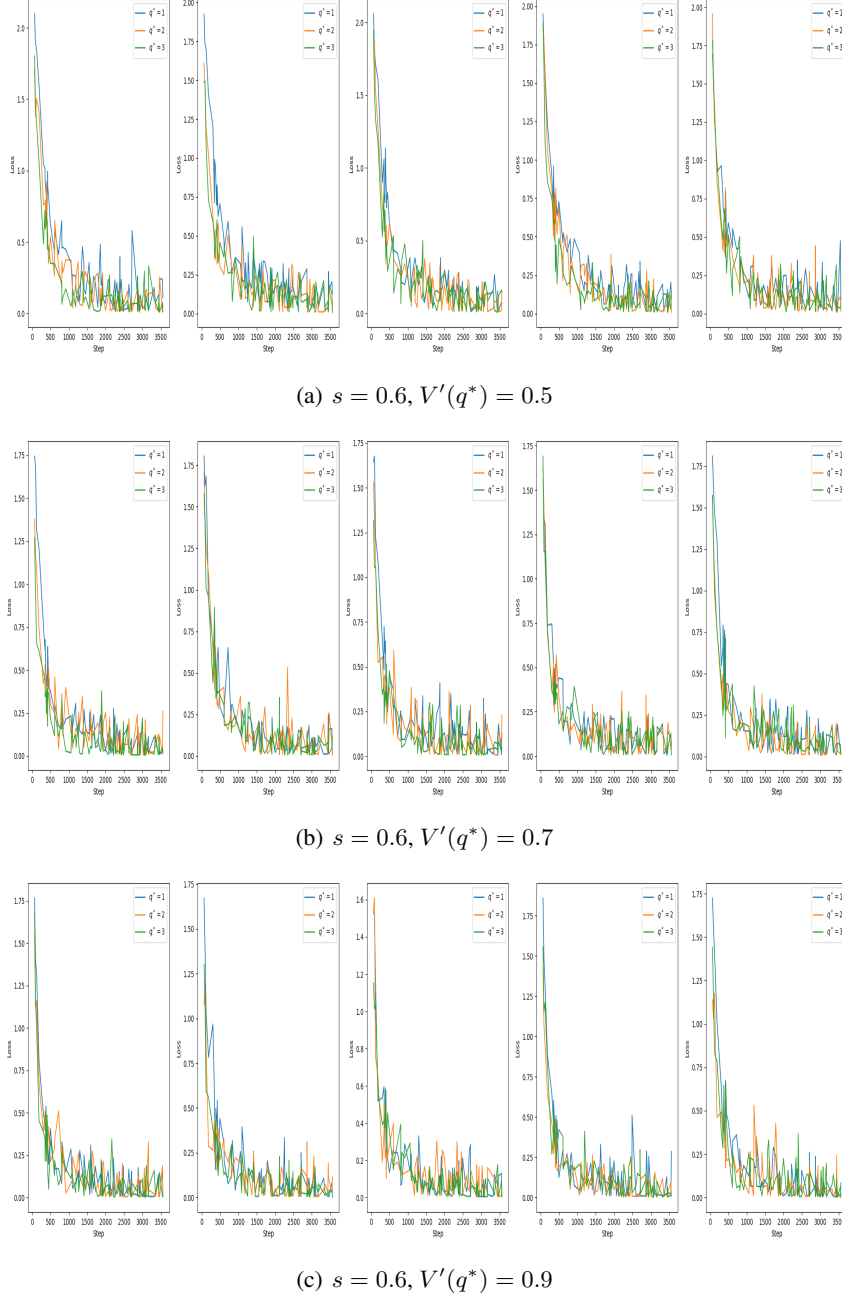
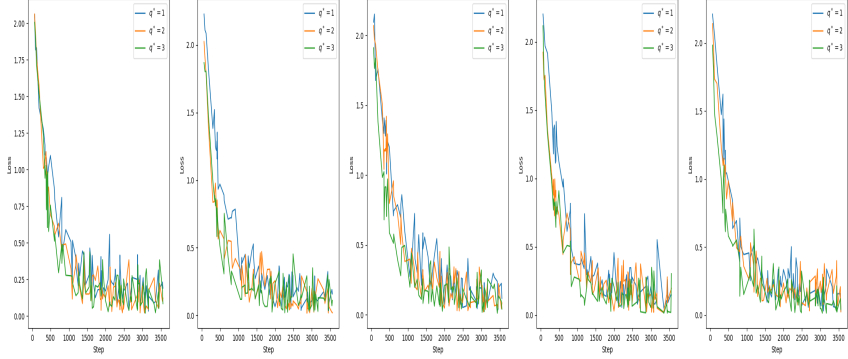
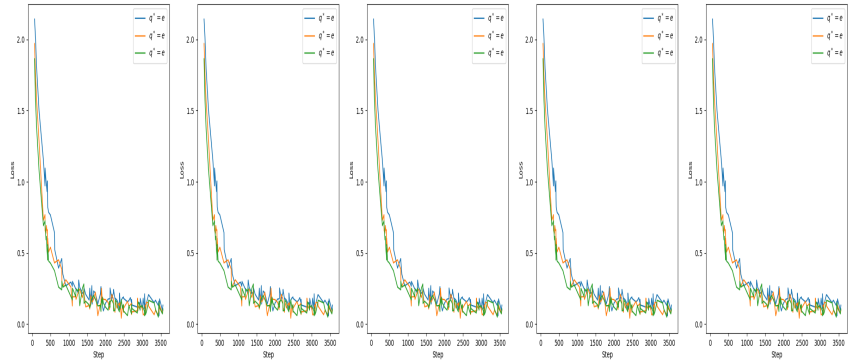


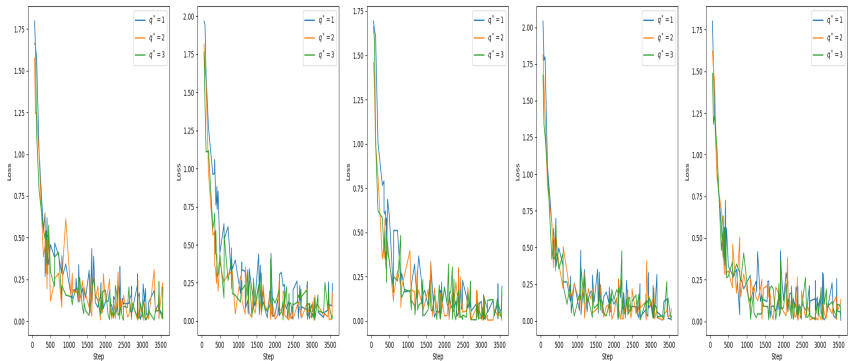
Figure 13: Training loss for a DNN depth 100 and width 300, trained on MNIST, batch size 64 and learning rate $\eta = 10^{-4}$, for activation function $\phi = \text{CReLU}_{\tau,m}$, with τ and m chosen such that $s = 0.6$, and for a given $V'(q^*)$.



(a) $s = 0.7, V'(q^*) = 0.5$

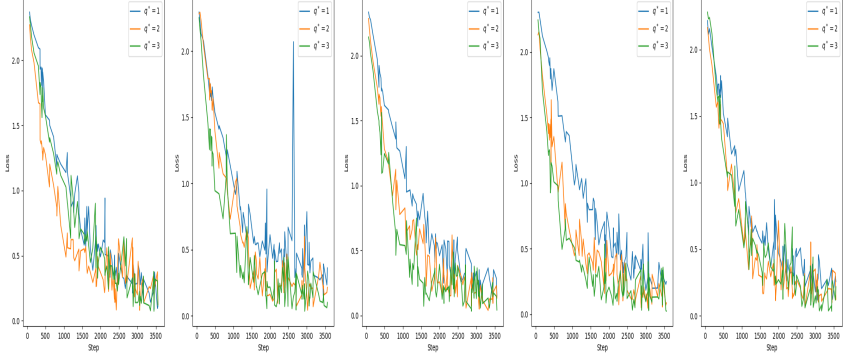


(b) $s = 0.7, V'(q^*) = 0.7$

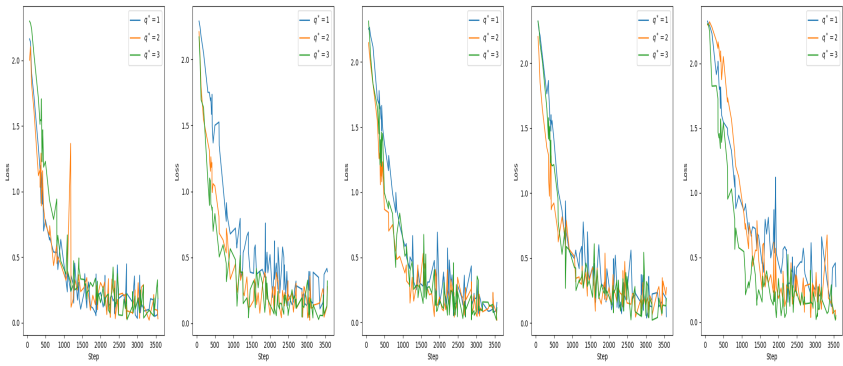


(c) $s = 0.7, V'(q^*) = 0.9$

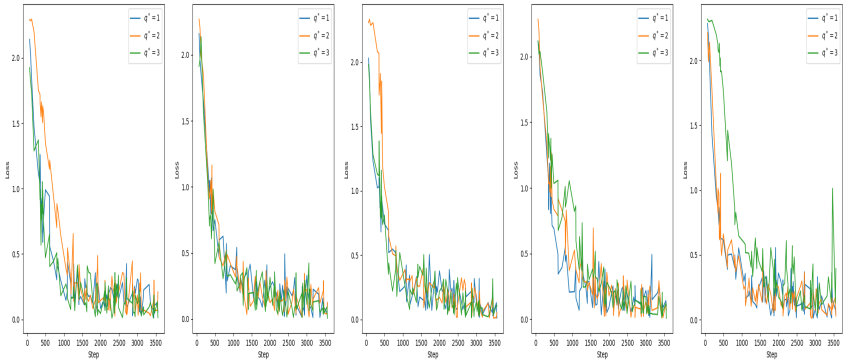
Figure 14: Training loss for a DNN depth 100 and width 300, trained on MNIST, batch size 64 and learning rate $\eta = 10^{-4}$, for activation function $\phi = \text{CReLU}_{\tau,m}$, with τ and m chosen such that $s = 0.7$, and for a given $V'(q^*)$.



(a) $s = 0.8, V'(q^*) = 0.5$

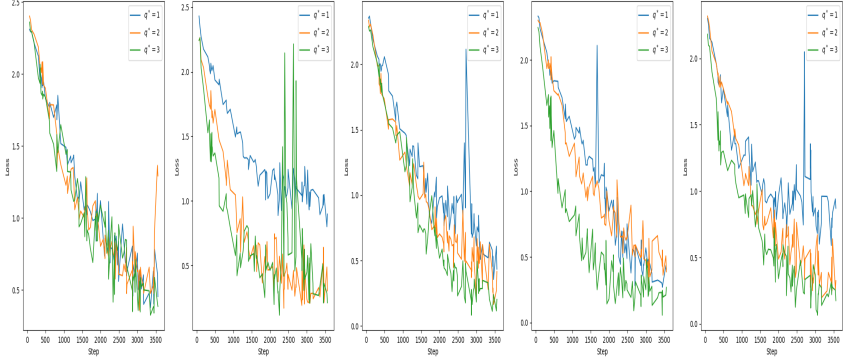


(b) $s = 0.8, V'(q^*) = 0.7$

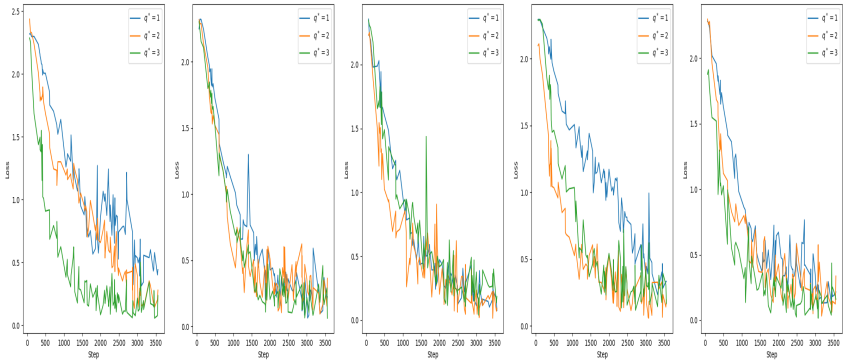


(c) $s = 0.8, V'(q^*) = 0.9$

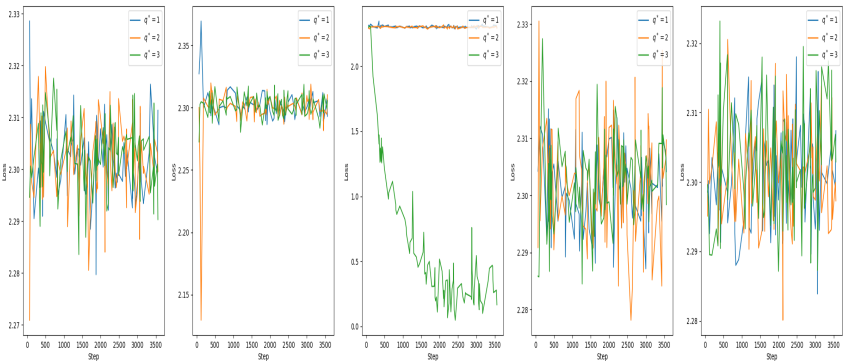
Figure 15: Training loss for a DNN depth 100 and width 300, trained on MNIST, batch size 64 and learning rate $\eta = 10^{-4}$, for activation function $\phi = \text{CReLU}_{\tau,m}$, with τ and m chosen such that $s = 0.8$, and for a given $V'(q^*)$.



(a) $s = 0.85, V'(q^*) = 0.5$

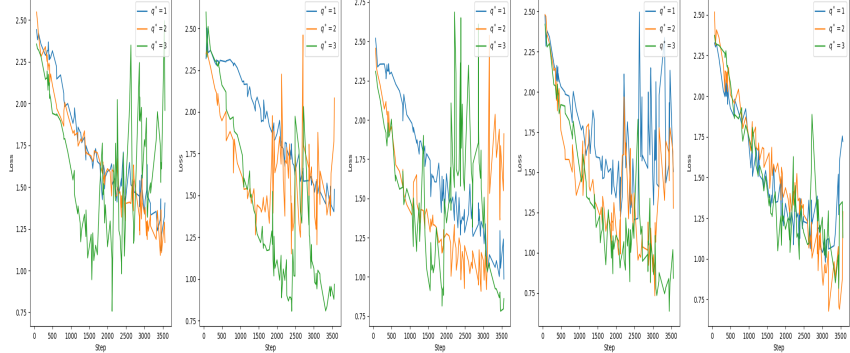


(b) $s = 0.85, V'(q^*) = 0.7$

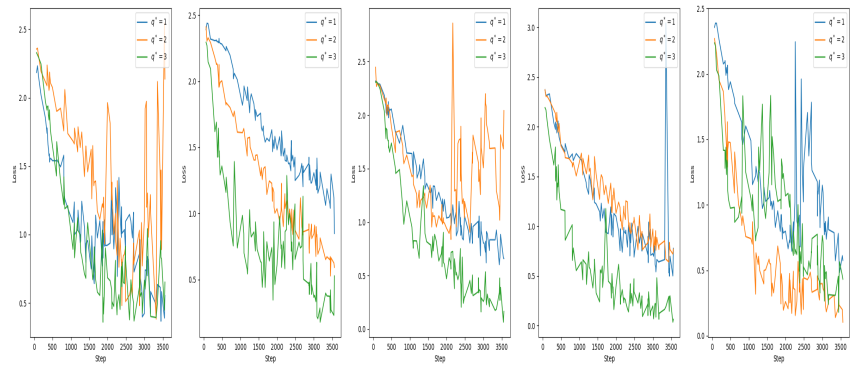


(c) $s = 0.85, V'(q^*) = 0.9$

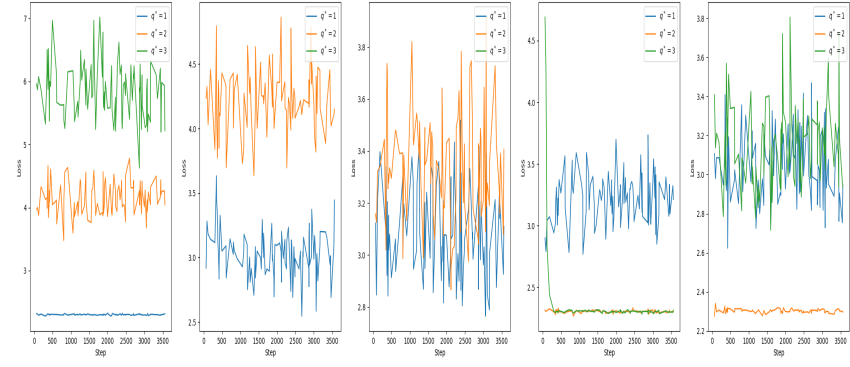
Figure 16: Training loss for a DNN depth 100 and width 300, trained on MNIST, batch size 64 and learning rate $\eta = 10^{-4}$, for activation function $\phi = \text{CReLU}_{\tau,m}$, with τ and m chosen such that $s = 0.85$, and for a given $V'(q^*)$.



(a) $s = 0.9, V'(q^*) = 0.5$



(b) $s = 0.9, V'(q^*) = 0.7$



(c) $s = 0.9, V'(q^*) = 0.9$

Figure 17: Training loss for a DNN depth 100 and width 300, trained on MNIST, batch size 64 and learning rate $\eta = 10^{-4}$, for activation function $\phi = \text{CReLU}_{\tau,m}$, with τ and m chosen such that $s = 0.9$, and for a given $V'(q^*)$.

E.2 $\text{CST}_{\tau,m}$

E.2.1 Summary Table

This section replicates many of the experiments from Section 3 but for the nonlinear activation $\text{CST}_{\tau,m}$ as defined in (2). Table 3 is analogous to Table 1. Note also that for desired sparsity level s with activation $\text{CST}_{\tau,m}$, set $\hat{\tau} = \sqrt{2q^*}\text{erf}^{-1}(s)$. Table 3 shows that generally, increased q^* allows for improved test accuracy where otherwise full accuracy could not be retained.

Table 3: DNN Trained on MNIST, 100 layers and 300 width, using activation function $\text{CST}_{\tau,m}$, batch size 64, results on 20% of data retained for testing. This was implemented using Pytorch Lightning over 200 epochs, with learning rate $\eta = 10^{-4}$.

DNN on MNIST														
		$q^* = 1$				$q^* = 2$				$q^* = 3$				
s	$V'(q^*)$	m	$V''(q^*)$	Accuracy	Sparsity	m	$V''(q^*)$	Accuracy	Sparsity	m	$V''(q^*)$	Accuracy	Sparsity	
$\text{CST}_{\tau,m}$	0.6	0.5	1.22	1.72	0.88	0.60	2.11	-0.14	0.88	0.60	-0.07	-0.05	0.88	0.60
		0.7	1.63	2.30	0.89	0.60	2.82	0.08	0.89	0.60	0.04	0.03	0.89	0.60
		0.9	2.25	3.18	0.89	0.60	3.89	0.40	0.90	0.57	0.20	0.13	0.74	0.53
	0.7	0.5	1.05	1.49	0.89	0.70	1.82	-0.05	0.87	0.70	-0.02	-0.02	0.88	0.70
		0.7	1.45	2.05	0.88	0.70	2.51	0.21	0.88	0.70	0.10	0.07	0.88	0.70
		0.9	2.05	2.90	0.27	0.42	3.56	0.58	0.11	0.31	0.29	0.19	0.58	0.50
	0.8	0.5	0.89	1.26	0.77	0.80	1.54	0.11	0.85	0.80	0.05	0.04	0.91	0.80
		0.7	1.27	1.79	0.89	0.80	2.19	0.41	0.89	0.80	0.20	0.14	0.89	0.80
		0.9	1.85	2.62	0.10	0.32	3.21	0.84	0.11	0.28	0.42	0.28	0.10	0.26
0.85	0.5	0.81	1.14	0.62	0.85	1.40	0.22	0.85	0.85	0.11	0.07	0.83	0.84	
		0.7	1.17	1.66	0.87	0.85	2.03	0.56	0.82	0.84	0.28	0.19	0.90	0.85
		0.9	1.74	2.46	0.10	0.62	3.01	1.05	0.10	0.51	0.52	0.35	0.10	0.41

E.2.2 Mean Training Loss Plots

Figure 18 shows the mean training loss for each parameter set of experiments of $\text{CST}_{\tau,m}$ across five seeds of a DNN. Figure 18 shows that, similarly to experiments for $\text{CReLU}_{\tau,m}$, there is improved training dynamics on average across parameter sets with increased q^* .

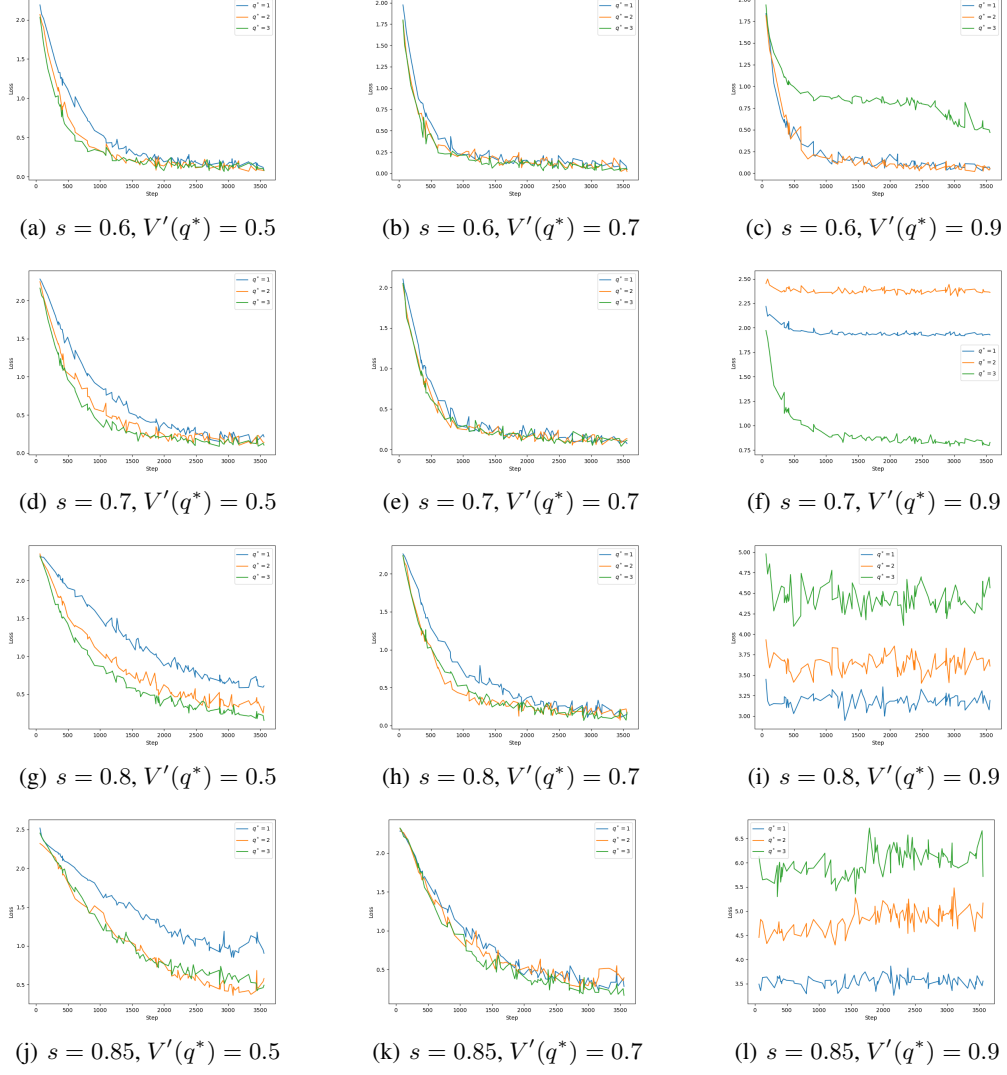


Figure 18: Mean training loss across 5 seeds for a DNN depth 100 and width 300, trained on MNIST, batch size 64 and learning rate $\eta = 10^{-4}$, for activation function $\phi = \text{CST}_{\tau,m}$, with τ and m chosen such that $s, V'(q^*)$ are as described.

E.2.3 Individual Run Training Loss Plots

Now Figures 19-22 show the training loss for each individual run of a DNN depth 100 and width 300 trained on MNIST. Figures 19-22 show the improved training speed across each individual run for increased q^* , in particular we see a recovery in ability to train for case $s = 0.7$, $V'(q^*) = 0.9$ for $\text{CST}_{\tau,m}$.

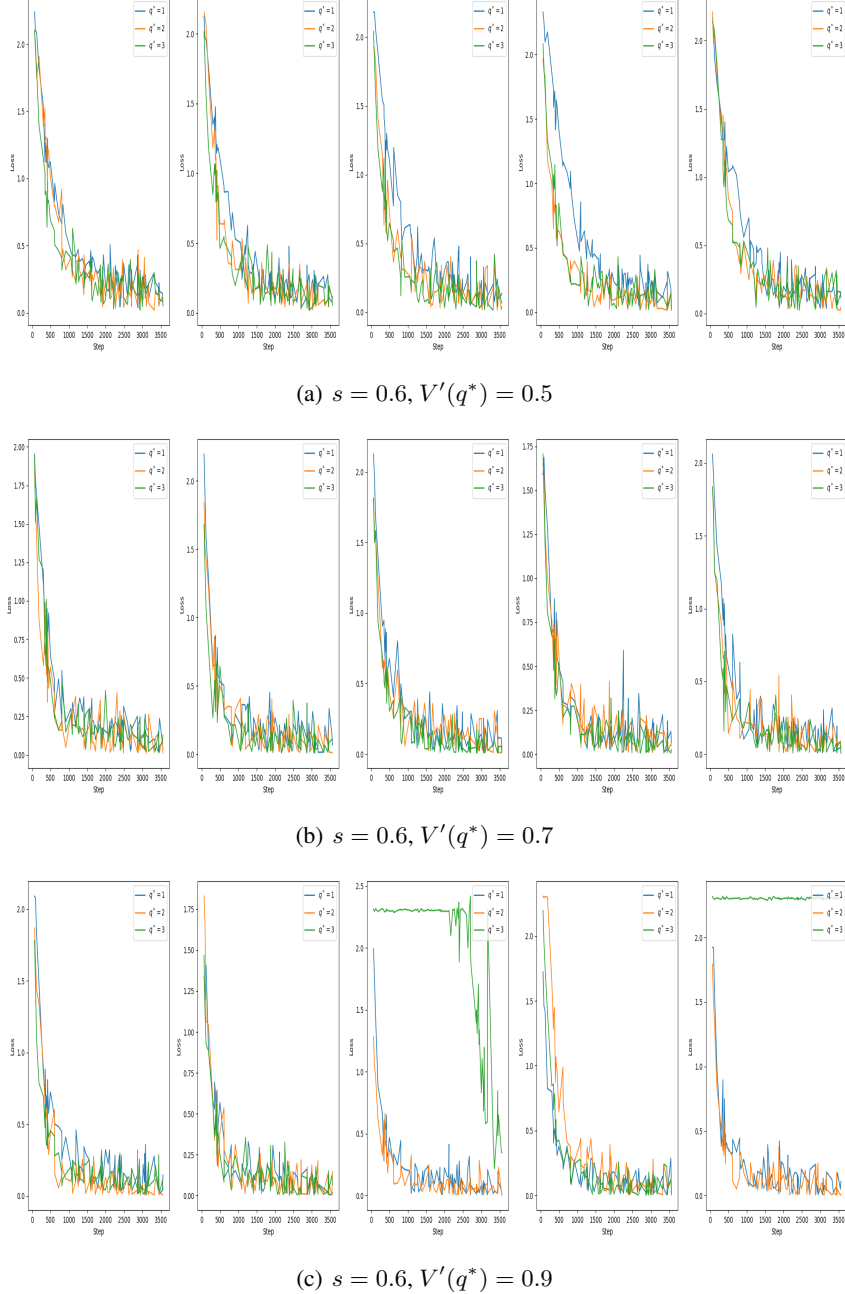
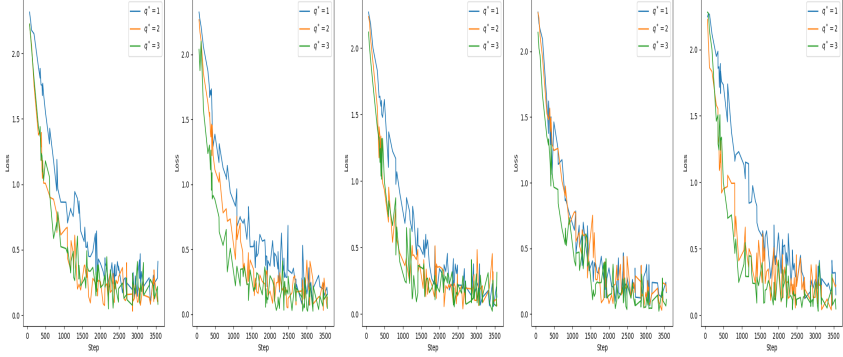
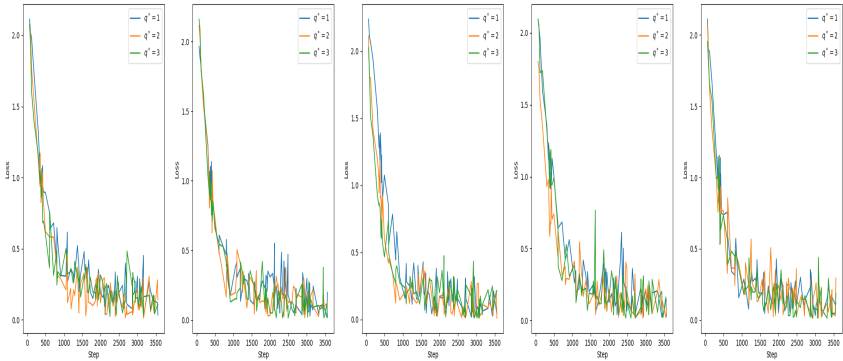


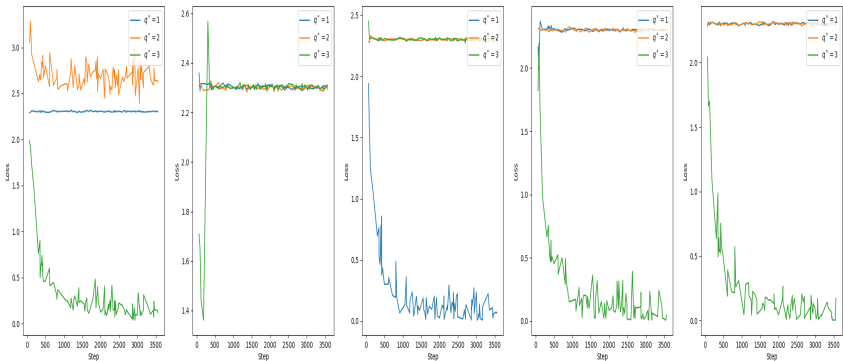
Figure 19: Training loss for a DNN depth 100 and width 300, trained on MNIST, batch size 64 and learning rate $\eta = 10^{-4}$, for activation function $\phi = \text{CST}_{\tau,m}$, with τ and m chosen such that $s = 0.6$, and for a given $V'(q^*)$.



(a) $s = 0.7, V'(q^*) = 0.5$

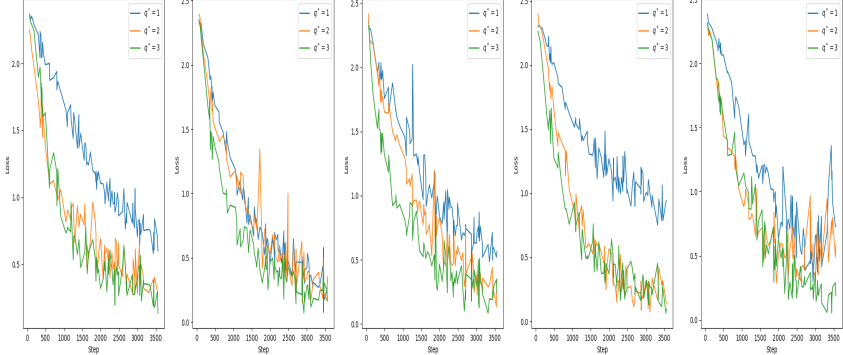


(b) $s = 0.7, V'(q^*) = 0.7$

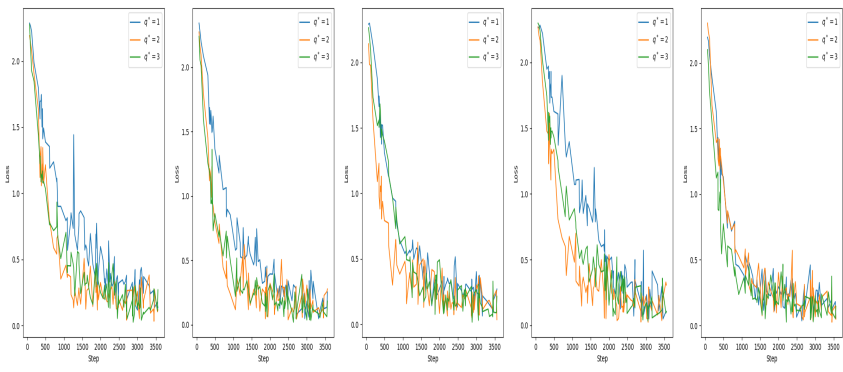


(c) $s = 0.7, V'(q^*) = 0.9$

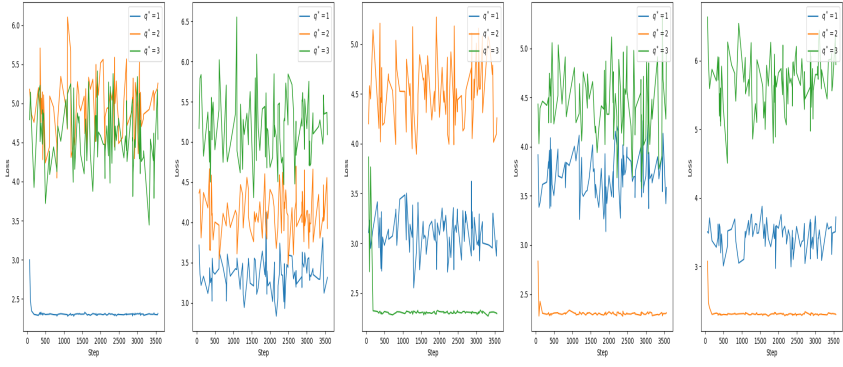
Figure 20: Training loss for a DNN depth 100 and width 300, trained on MNIST, batch size 64 and learning rate $\eta = 10^{-4}$, for activation function $\phi = \text{CST}_{\tau,m}$, with τ and m chosen such that $s = 0.7$, and for a given $V'(q^*)$.



(a) $s = 0.8, V'(q^*) = 0.5$

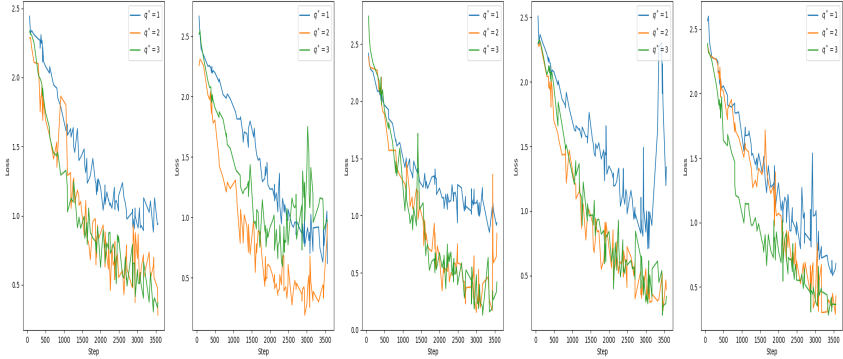


(b) $s = 0.8, V'(q^*) = 0.7$

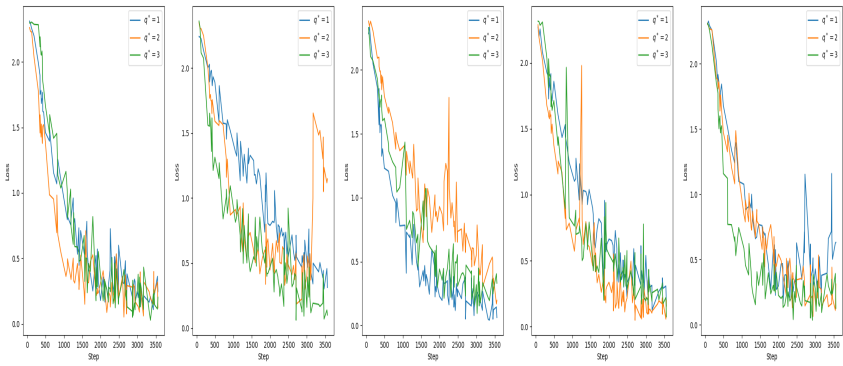


(c) $s = 0.8, V'(q^*) = 0.9$

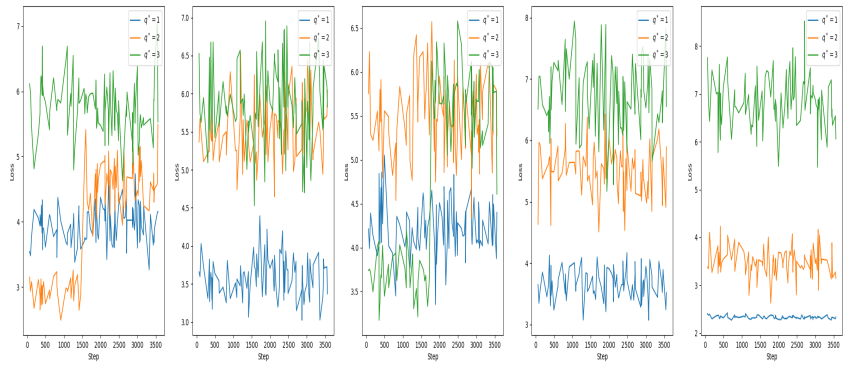
Figure 21: Training loss for a DNN depth 100 and width 300, trained on MNIST, batch size 64 and learning rate $\eta = 10^{-4}$, for activation function $\phi = \text{CST}_{\tau,m}$, with τ and m chosen such that $s = 0.8$, and for a given $V'(q^*)$.



(a) $s = 0.85, V'(q^*) = 0.5$



(b) $s = 0.85, V'(q^*) = 0.7$



(c) $s = 0.85, V'(q^*) = 0.9$

Figure 22: Training loss for a DNN depth 100 and width 300, trained on MNIST, batch size 64 and learning rate $\eta = 10^{-4}$, for activation function $\phi = \text{CST}_{\tau,m}$, with τ and m chosen such that $s = 0.85$, and for a given $V'(q^*)$.

F Further CNN Experiment Results

This section provides further figures for experiments of CNNs on the training loss behaviour of increasing q^* for $\phi = \text{CReLU}_{\tau,m}$, summarised in Section 3. Due to larger variability in training loss at each step the mean training loss across seeds is uninformative and hence Figures 23-27 show individual runs training loss, and generally demonstrate improved training dynamics for larger q^* .

F.1 Individual Run Training Loss Plots

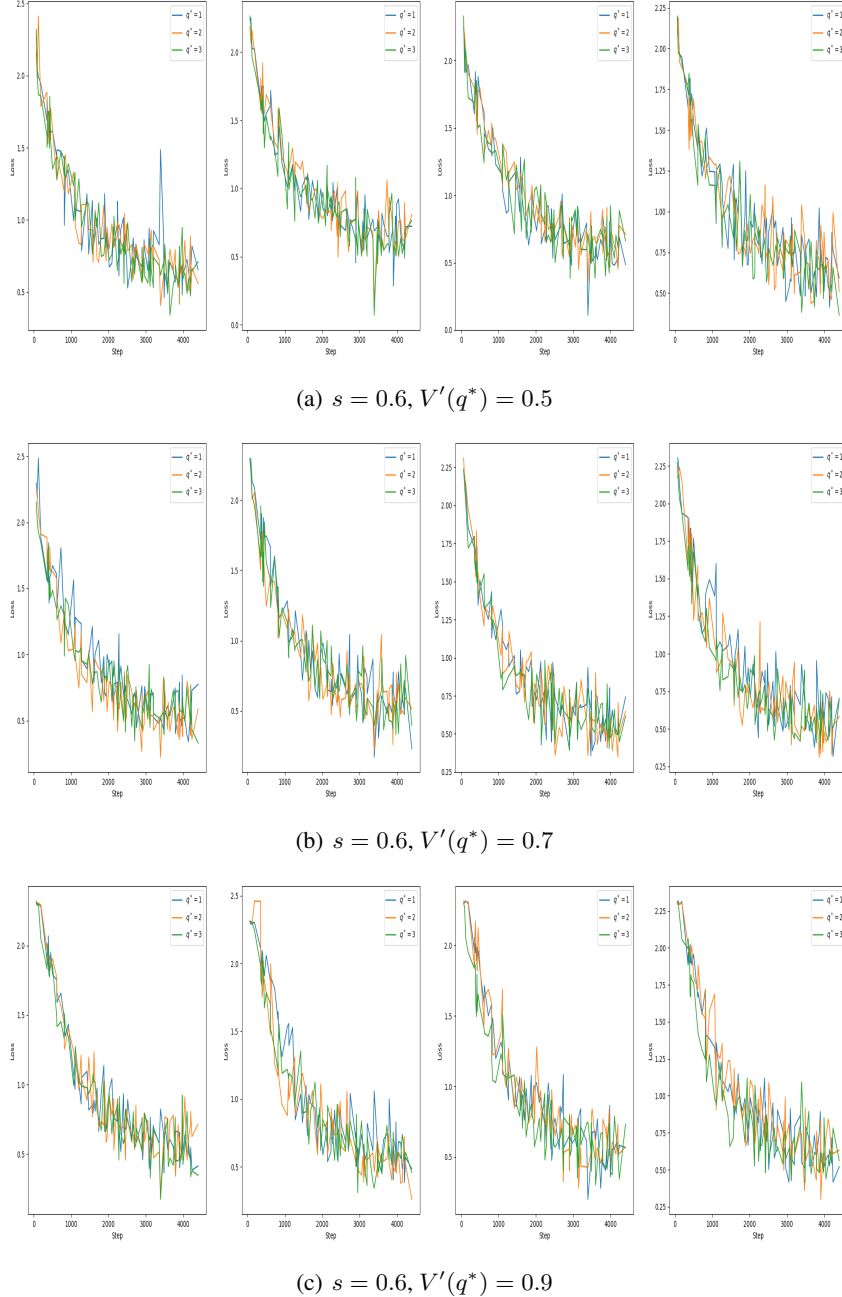
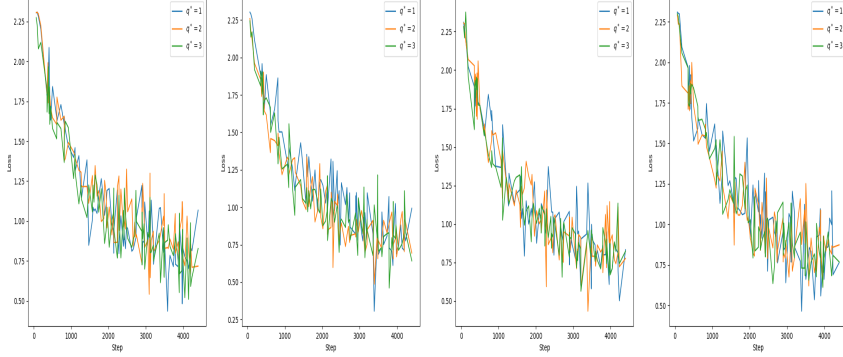
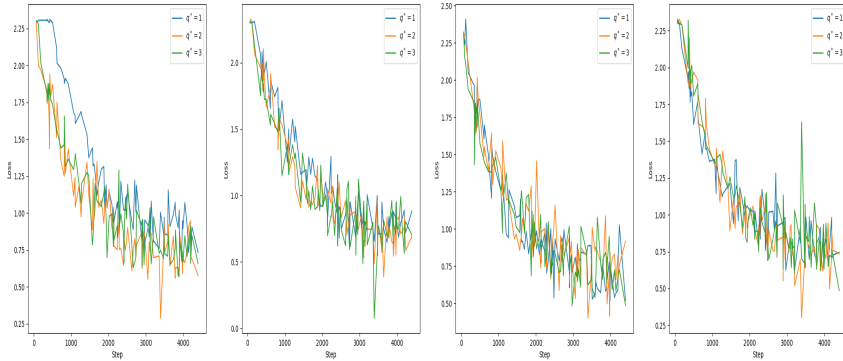


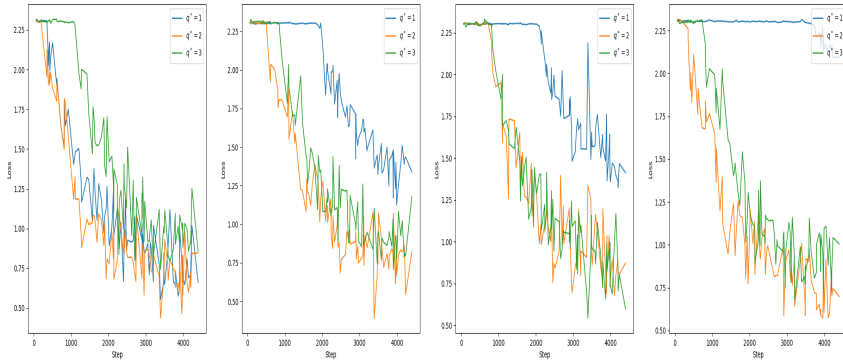
Figure 23: Training loss for a CNN depth 50 and 300 channels per layer, trained on CIFAR10, batch size 64 with learning rate $\eta = 10^{-3}$ and cosine learning rate schedule, for activation function $\phi = \text{CReLU}_{\tau,m}$, with τ and m chosen such that $s = 0.6$, and for a given $V'(q^*)$.



(a) $s = 0.7, V'(q^*) = 0.5$

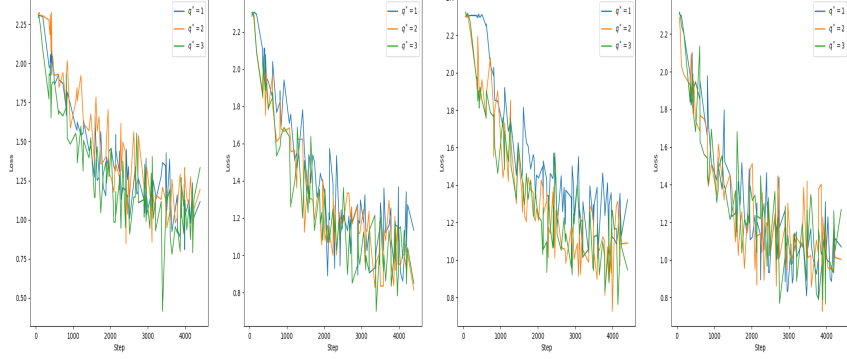


(b) $s = 0.7, V'(q^*) = 0.7$

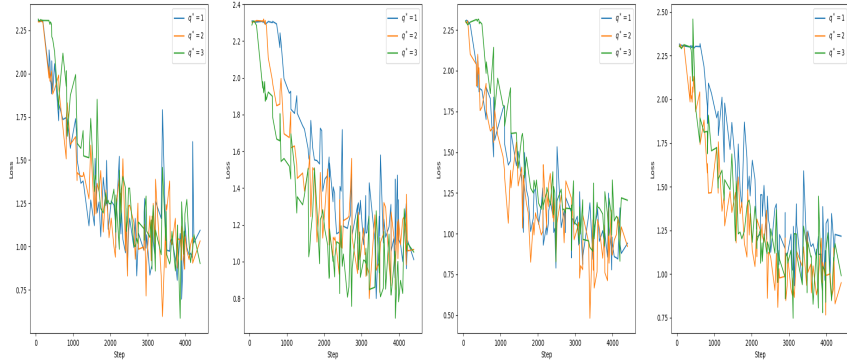


(c) $s = 0.7, V'(q^*) = 0.9$

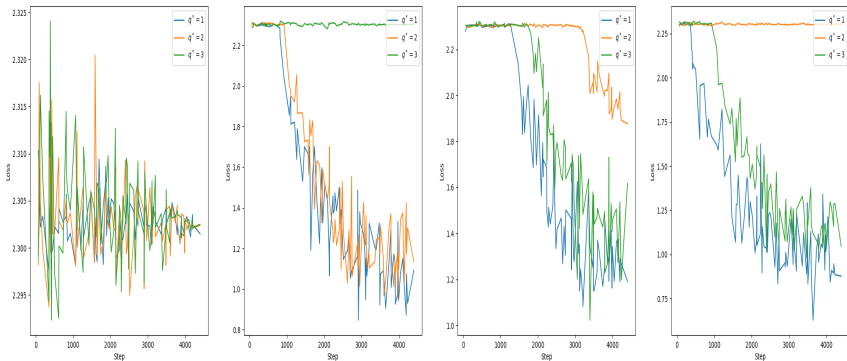
Figure 24: Training loss for a CNN depth 50 and 300 channels per layer, trained on CIFAR10, batch size 64 with learning rate $\eta = 10^{-3}$ and cosine learning rate schedule, for activation function $\phi = \text{CReLU}_{\tau,m}$, with τ and m chosen such that $s = 0.7$, and for a given $V'(q^*)$.



(a) $s = 0.8, V'(q^*) = 0.5$

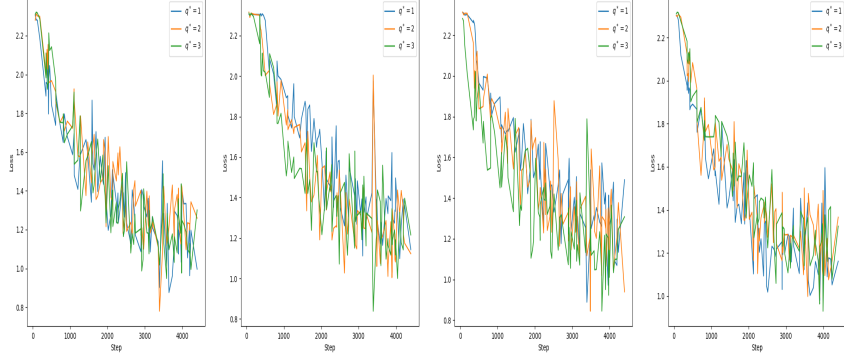


(b) $s = 0.8, V'(q^*) = 0.7$

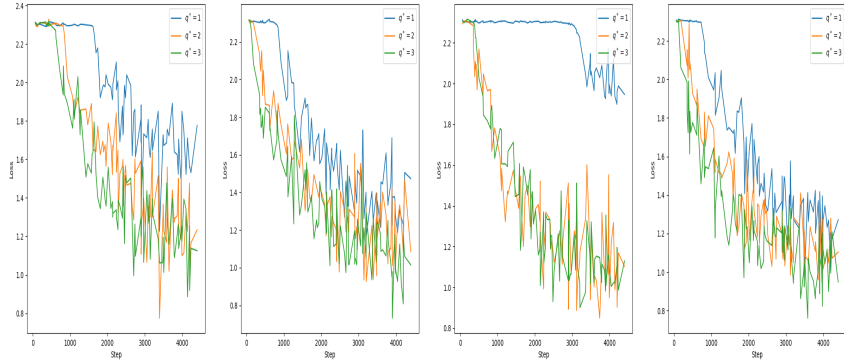


(c) $s = 0.8, V'(q^*) = 0.9$

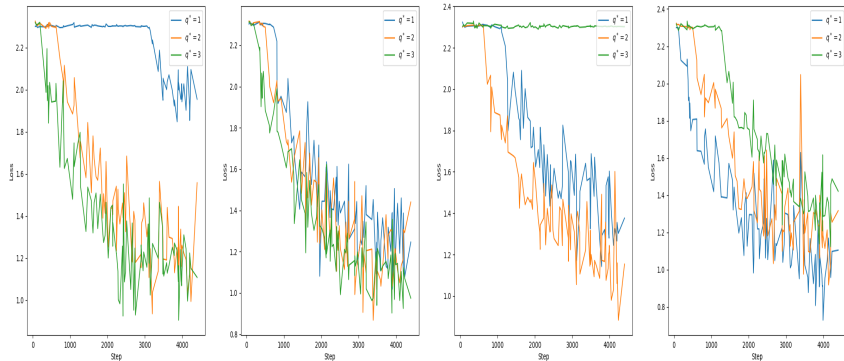
Figure 25: Training loss for a CNN depth 50 and 300 channels per layer, trained on CIFAR10, batch size 64 with learning rate $\eta = 10^{-3}$ and cosine learning rate schedule, for activation function $\phi = \text{CReLU}_{\tau,m}$, with τ and m chosen such that $s = 0.8$, and for a given $V'(q^*)$.



(a) $s = 0.85, V'(q^*) = 0.5$

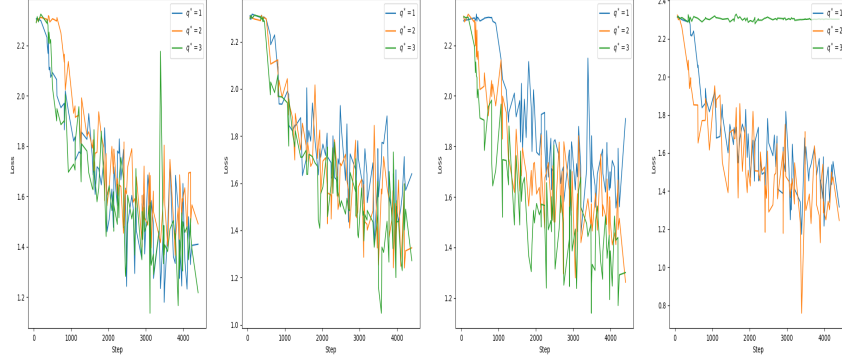


(b) $s = 0.85, V'(q^*) = 0.7$

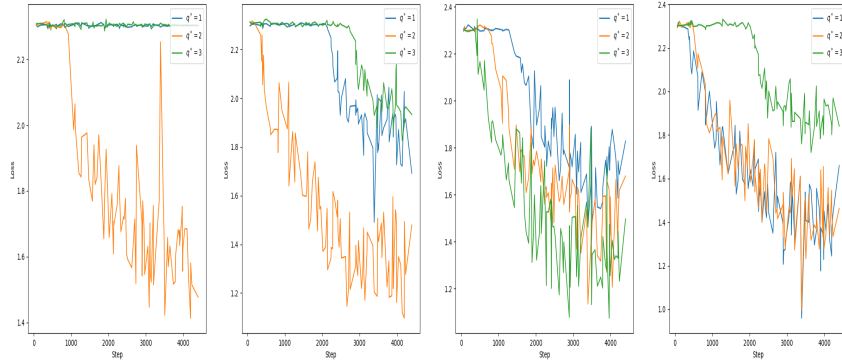


(c) $s = 0.85, V'(q^*) = 0.9$

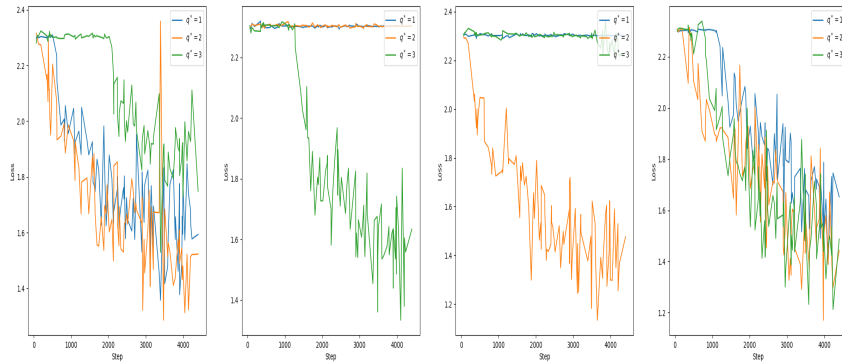
Figure 26: Training loss for a CNN depth 50 and 300 channels per layer, trained on CIFAR10, batch size 64 with learning rate $\eta = 10^{-3}$ and cosine learning rate schedule, for activation function $\phi = \text{CReLU}_{\tau,m}$, with τ and m chosen such that $s = 0.85$, and for a given $V'(q^*)$.



(a) $s = 0.9, V'(q^*) = 0.5$



(b) $s = 0.9, V'(q^*) = 0.7$



(c) $s = 0.9, V'(q^*) = 0.9$

Figure 27: Training loss for a CNN depth 50 and 300 channels per layer, trained on CIFAR10, batch size 64 with learning rate $\eta = 10^{-3}$ and cosine learning rate schedule, for activation function $\phi = \text{CReLU}_{\tau,m}$, with τ and m chosen such that $s = 0.9$, and for a given $V'(q^*)$.